UNIVERSITAT DE BARCELONA

# Immunoreceptor MerTK: A journey from the membrane into the nucleus of human dendritic cells

Kyra J. E. Borgman

# Part I:

# Novel biophysical tools in nano-immunology

# Novel biophysical techniques in nano-immunology

**The rapid spread of nanotechnology and nanoscience in different fields of science has recently lead to the new emerging field of nano-immunology. Novel microscopy techniques and biophysical tools for the visualization of molecular events at the nanoscale in immune cells, as well as novel nanoparticles that interact with immune cells to modulate an immune response, are becoming readily accessible tools to immunologists. In here, we discuss several advanced imaging techniques which are important in nano-immunology. These imaging techniques aid, in different ways, in accessing molecular information at the nanometre scale. For each technique, an example of how we used this tool to address specific questions within the field is discussed.**

The work discussed here is part of the following publications:

---


- Piechocka IK, Sosa-Costa A, Mohan N, **Borgman KJE**, Keary S, Lakadamyali M, Manzo C, Garcia-Parajo MF, *Shear flow driven actin reorganization promotes ICAM-1 nanoclustering on endothelial cells effecting T-cell migration.* Submitted to J. Cell Sci.

- Porto V, Borrajo E, Buceta D, Carneiro C, Huseyinova S, Domínguez B, **Borgman KJE**, Lakadamyali M, Garcia-Parajo MF, Neissa J, Garcia-Caballero T, Barone G,. Blanco C, Busto N, García B, Leal J M, Blanco J, Rivas J, López- Quintela A and Domínguez F*, Silver atomic quantum clusters of three atoms for cancer therapy: targeting chromatin compaction to increase the therapeutic index of chemotherapy*. Advanced Materials 1801317 2018

- Sosa-Costa A, Isern de Val S, Sevilla-Movilla S, **Borgman KJE**, Marzo C, Teixidó J, Garcia-Parajo MF, *Lateral Mobility and Nanoscale Spatial Arrangement of Chemokine-activated α4β1 Integrins on T Cells.* J Biol Chem 291(40) 2016

- Regmi R, Winkler PM, Frauraud V, **Borgman KJE**, Manzo C, Brugger J, Rignault H, Wenger J, Garcia-Parajo MF, *Planar optical nanoantennas resolve cholesterol-dependent nanoscale heterogeneities in the plasma membrane of living cells*. Nanoletters 17(10) 2017

- **Borgman KJE**, Zanten TS van, Manzo C, Cabezón R, Cambi A, Benítez-Ribas D, Garcia-Parajo MF, *Priming by chemokines restrict lateral mobility of the adhesion receptor LFA-1 and restores adhesion to ICAM-1 nano-aggregates on human mature dendritic cells.* PLoS ONE 9(6) 2014

# I.1 Introduction

An adequate immune reaction starts with discriminating non-self, threatening antigens from the body's own, self material[1]. Frequent interactions between immune cells and other cells, immune cells and the environment and immune cells amongst each other are crucial in this process. These interactions start at the level of the cell membrane and therefore membrane biology is playing a very important role within the field. Classically, immune cells are characterized by the membrane proteins that they express, i.e., immunophenotyping[2]. This is commonly performed by flow cytometry, a technique that allows for the identification, description and quantification of subpopulations in a cell suspension using fluorescently labelled antibodies. Flow cytometry has allowed the detection of phenotypical changes and abnormalities in malignancies[3,4] and other diseases[5,6]. The extremely high-throughput and sensitivity for very small imbalances in subpopulations have made immunophenotyping by flow cytometry an immensely popular tool in immunology over the last few decades[7].

The high-throughput making flow cytometry as popular as it is nowadays however comes at a price. The information gained remains extremely descriptive, and fails to provide the molecular mechanisms of action of the immunoreceptors stained. Important characteristics to investigate in order to understand the behaviour of membrane receptors are: *a)* their localization at the micrometric and organization at the nanometric scale, *b)* their dynamic behaviour and, *c)* their positioning relative to and interaction with other proteins. Optical techniques have the great advantage of being able to access all of this information due to a combination of chemical specificity coming from fluorescent labelling, and their non-invasive character compatible with live-cell imaging. To go beyond a descriptive picture towards a more functional understanding of these biomolecules, a sophisticated, quantitative analysis of the acquired data is crucial.

Classical wide-field and confocal microscopy has greatly advanced our understanding in life sciences at the micrometre scale allowing for example the visualization of cellular organelles or bacteria. However, information at the nanoscale including individual protein complexes or the structure of chromatin is lacking behind. In 1873, Ernst Abbe described how light based optical microscopy is fundamentally limited by diffraction[8]. He postulated that two objects closer to each other than half of the wavelength of light can never be resolved optically. In the case of fluorescence microscopy within the visible range, this means that the lateral resolution limit is around 250 nm. Especially in the crowed environment of the cell membrane, with transmembrane proteins that are typically 1-10 nm in size and are expressed at very high density levels of 1000-2000 proteins/$\mu$m$^2$ [9], the resolution limit hampers full understanding of the molecular landscape. In section

I.2, we will discuss two newly emerged imaging techniques that are able to break the diffraction limit of light, allowing the direct visualization of how biomolecules are organized at the nanoscale.

Although able to break the diffraction limit and gain high spatial resolution, these novel imaging techniques are inherently slow and lack behind in temporal resolution. Complementary approaches to inquire on the dynamic behaviour of biomolecules are therefore of equal importance in order to get a full picture of their molecular mechanism of action. In section I.3, we will discuss two novel biophysical tools that are instrumental in determining the dynamic profile of biomolecules with very high temporal resolution up to the μs range.

The cell is a very crowed place and biomolecules do not function individually. It is therefore very important to additionally study the interaction between different molecules. Scaling the techniques mentioned above up to imaging 2 or 3 molecules at the same time labelled in different colours is a great approach to gain more information on their behaviour relative to each other. In section I.4, we will additionally discuss an innovative approach to study the direct interaction between proteins using microfabrication techniques.

Below, the fundamental principles of these novel biophysical tools, the quantitative analysis associated to them, and their specific advantages in the field of nano-immunology are discussed. Additionally, an example of how each of these techniques have been exploited to answer specific biological questions in the field is given. All examples presented are publications that I co-authored during my doctoral studies.

# I.2 Super-resolution microscopy breaking the diffraction limit

### STED - Stimulated emission depletion

In 1994, Stefan Hell published his first theoretical paper on using stimulated emission as a way to enhance the resolution of the optical microscope[10]. In this approach, two different laser beams of different wavelengths are combined: one beam that excites fluorescent molecules, and another beam that depletes their spontaneous fluorescence through stimulated emission. During spontaneous emission, a fluorophore is excited from the ground state ($S_0$) to the excited state ($S_1$) by a photon of a certain wavelength $\lambda$

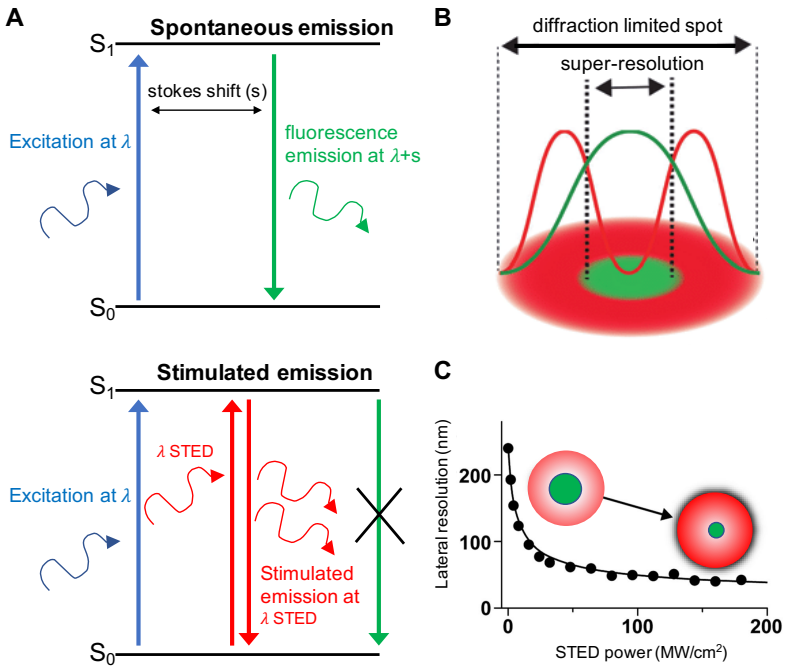


**Figure I.1: STED principle explained.** (**A**) Upper panel: A fluorophore is excited from the ground state ($S_0$) to the excited state ($S_1$) by a photon of a certain wavelength $\lambda$. The fluorophore spontaneously decays back to the ground state by emitting a photon with of a red-shifted wavelength ($\lambda$+s), a process called spontaneous emission. Lower panel: While being in the excited state, the molecule can absorb another photon from a second (red-shifted) excitation laser. This second photon will force the excited molecule to the ground state without the emission of a fluorescent photon, i.e., stimulated emission depletion. (**B**) STED nanoscopy takes advantage of stimulated emission to effectively reduce the width of the excitation beam. This is done by overlaying a donut-shaped STED beam with a diffraction limited excitation beam, where the maximum of the excitation beam coincides with the zero-intensity centre of the STED beam. (**C**) Theoretical dependence of the lateral resolution obtained with STED nanoscopy as a function of the power of the depletion laser[11]. The green circles on the plot illustrate the effective resolution obtained. For low STED intensity powers, the gain in resolution is poor. Increasing the STED power will result in an effective small illumination spot and increased super-resolution.

(Figure I.1 A). The fluorophore then spontaneously decays back to the ground state while emitting a photon with of a red-shifted wavelength ($\lambda$+s). This is in fact the normal process of fluorescence and in fluorescence microscopy, this shift allows one to separate the fluorescently emitted photons from the excitation laser to generate a fluorescence image. During stimulated emission on the other hand, a second laser is impinged on the fluorescence molecule while it is in the excited state, i.e., before it decays via fluorescence. This causes the emission of two photons, i.e., stimulated emission. However, these emitted photons have the same wavelength of the second laser used for stimulated emission and as a result, the emission of fluorescence photons is inhibited (Figure I.1 A). Thus, in a trivial implementation when one simultaneously excites a molecule with these two lasers, no fluorescence will ever be emitted. The key in STED nanoscopy is to take advantage of this depletion of the fluorescence emission to effectively reduce the width of the excitation beam and thereby break the diffraction limit. This is done by overlaying the standard excitation laser used for fluorescence with a donut-shaped STED laser beam that has zero intensity in the centre of the donut (Figure I.1 B). The wavelength of the STED beam is red-shifted compared to the excitation beam and falls in the tail of the fluorophore's emission spectrum. When a sample of fluorophores is illuminated with the combination of both beams, the molecules in the centre of the donut will freely fluoresce since in this region only the excitation beam exists. At the same time, the fluorescence emission coming from the molecules in the donut region will be completely depleted through stimulated emission since in here both excitation and STED beams are present. The excitation beam has thus been effectively reduced in lateral size to the diameter of the zero-intensity centre of the STED beam (Figure I.1 B).

Ultimately, the resolution of STED microscopy with a given numerical aperture objective and excitation wavelength only depends on the intensity of the depletion beam together with the dye properties, and is therefore no longer diffraction limited (Figure I.1 C). Currently, in the optimal case of ultra-stable emitters such as diamond colour centres, STED can achieve an impressive resolution of around 6 nm[12]. However, in common applications for fixed cell imaging the attainable resolution is between 50-100nm. This is mainly due to the fact that the STED beam has to exhibit extreme laser power in order to favour stimulated emission over fluorescence emission and thus efficiently deplete fluorescence emission within the donut region. This high laser power can lead to heat damage to the sample, as well as significant photobleaching of the fluorescent dye used. Developing strategies to reduce the effective power needed[13–16] as well as the development of fluorescent dyes with favourable properties[17] are therefore active subjects of interest within the field of STED nanoscopy.

Of specific interest for this thesis is the use of STED nanoscopy in deciphering the nanoscale organization of immunoreceptors at the plasma membrane. Nanoclustering has been proposed as a dominant feature in the organization of the plasma membrane[18], and there are many examples where this also holds for immunoreceptors, such as the integrin LFA-1[19], the BCR[20] and TCR[21], pathogen recognition receptor DC-SIGN[22] and CD1d[23]. For the latter two examples, STED nanoscopy has been the main technique to uncover and characterize this organization at the nanoscale. In order to quantify the number of receptors contained in each nanocluster, the most common approach includes measuring the brightness of individual fluorescent spots on the cell membrane from multiple images on different cells. In order to obtain stoichiometric measurements, i.e., the number of molecules contained in each nanocluster, a reference fluorescence signal from individual antibodies is then required. This can be obtained by measuring the brightness of individual fluorescent spots of non-specifically adsorbed antibodies scarcely found on the substrate next to the cell surface. Their average intensity is then used to quantify the number of molecules contained in each spot. This quantification strategy has also been used in the example described below.

STED nanoscopy is a very well suited technique to study nanoclusters of immunoreceptors on the cell membrane, mainly due to its combination of reasonably high resolution together with fast and easy image acquisition. In the example studies mentioned here, the resolution of our STED system was around 80-100 nm. In contrast to other super-resolution techniques, STED imaging is very fast and requires little post-imaging processing, which makes it a well-suited technique for experiments where many images are required. That is certainly the case for reliable characterization of nanoclusters on the surface of primary immune cells, where not only cluster-to-cluster and cell-to-cell variability but also donor-to-donor variability needs to be considered. In the following example, the use of STED nanoscopy in the characterization of ICAM-1 nanoclusters on the membrane of endothelial cells is described.

*Shear flow driven actin reorganization promotes ICAM-1 nanoclustering on endothelial cells effecting T-cell migration*

Endothelial cells (ECs) form a natural barrier for regulating leukocyte migration within blood vessels. Leukocyte extravasation from the bloodstream to sites of inflammation or peripheral lymphoid organs involves a cascade of steps of leukocyte interactions with the activated endothelium. This multistep process initially includes low-affinity adhesive interactions (capture and rolling)[24], followed by firm adhesion[25], cell spreading and crawling[26], and finally leukocyte diapedesis through the endothelial barrier to the sites of

inflammation[27,28]. The mechanism of leukocyte firm adhesion to the endothelium and subsequent migration is mainly mediated by specific interactions between the ligand intracellular adhesion molecule-1 (ICAM-1) expressed by ECs and its leukocyte counter-receptor, the αLβ2 integrin lymphocyte function-associated antigen LFA-1[29,30].

Due to their localization on the EC surface, ICAM-1 molecules are continuously exposed *in vivo* to fluid shear stresses generated by blood flow. These ligands therefore not only have to withstand traction forces exerted by crawling leukocytes but also have to resist forces generated by flowing blood. It has been previously shown that shear force has an impact on ECs by upregulating the expression level of ICAM-1[31,32], modulating gene regulation[33,34], inducing cell shape and actin cytoskeleton organization[35], focal adhesion formation[36] and changes in membrane fluidity[37,38]. This leads to increased leukocyte binding to endothelium[31,39] and reinforcement of the initially created integrin-ligand bonds[40,41], which in turn promotes trans-endothelial migration[42].

Although the influence of shear forces on ECs has been studied extensively, the direct effect of forces on the spatial distribution of adhesion molecules on the apical EC surface prior to leukocyte adhesion has received less attention. To address this question, we pre-exposed inflammatory challenged (TNF-α-stimulated) ECs to continuous shear flow and followed over time the spatial distribution of ICAM-1 using confocal imaging. In the pre-

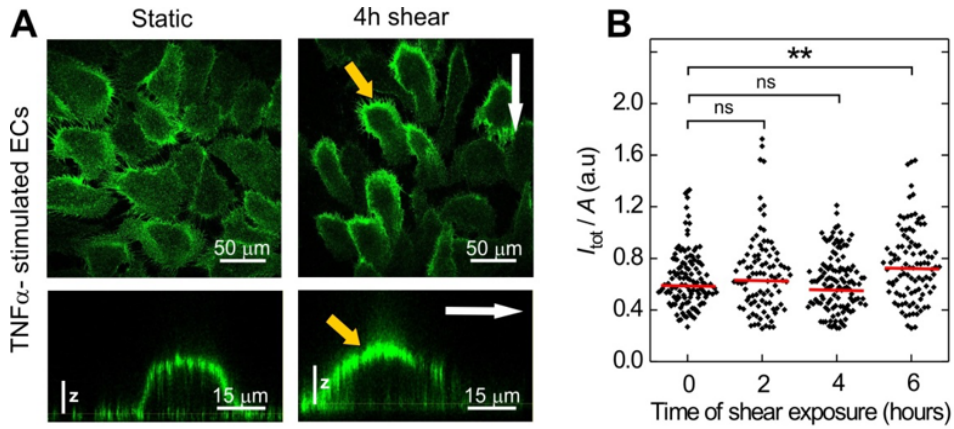


**Figure I.2 Effect of shear flow on TNF-α stimulated ECs. (A)** Single plane confocal microscopy images taken at the basal cell membrane (*top rows*) and 3*D* orthogonal views *(bottom rows*) of ICAM-1 expressed on TNF-α stimulated ECs, in absence of shear flow (*left column*) and after 4h of continuous flow application (*right column*). White arrows indicate the direction of shear flow while yellow arrows point at the upstream accumulation of ICAM-1. **(B)** Fluorescence intensity of the ICAM-1 signal integrated over the entire cell and normalized to the cell area, for static conditions (0 h) and for different times of shear exposure (2, 4 and 6 h). In total, 100 to 180 ECs from two separate experiments were analysed per condition. A flow of 8 dyn/cm$^2$ was applied.

-sence of shear flow, TNF-α-stimulated ECs become elongated and aligned along the flow direction while in static conditions cells were randomly oriented (Fig. I.2 A)**,** white arrow indicates the direction of the flow). A very strong ICAM-1 signal becomes furthermore apparent at the upstream side of the cells opposing the flow. Since the total expression levels of ICAM-1 are not effected in this case (Fig. I.2 B), we thus conclude that ICAM-1 undergoes a massive redistribution on ECs as early as 4 hours after the induction of shear flow.

To further investigate the ICAM-1 rearrangement at the nanometre scale, we imaged static as well as 4h shear-stimulated ECs using super-resolution STED nanoscopy (Fig.I.3 A). Individual fluorescent spots are clearly resolved in all conditions, although there were

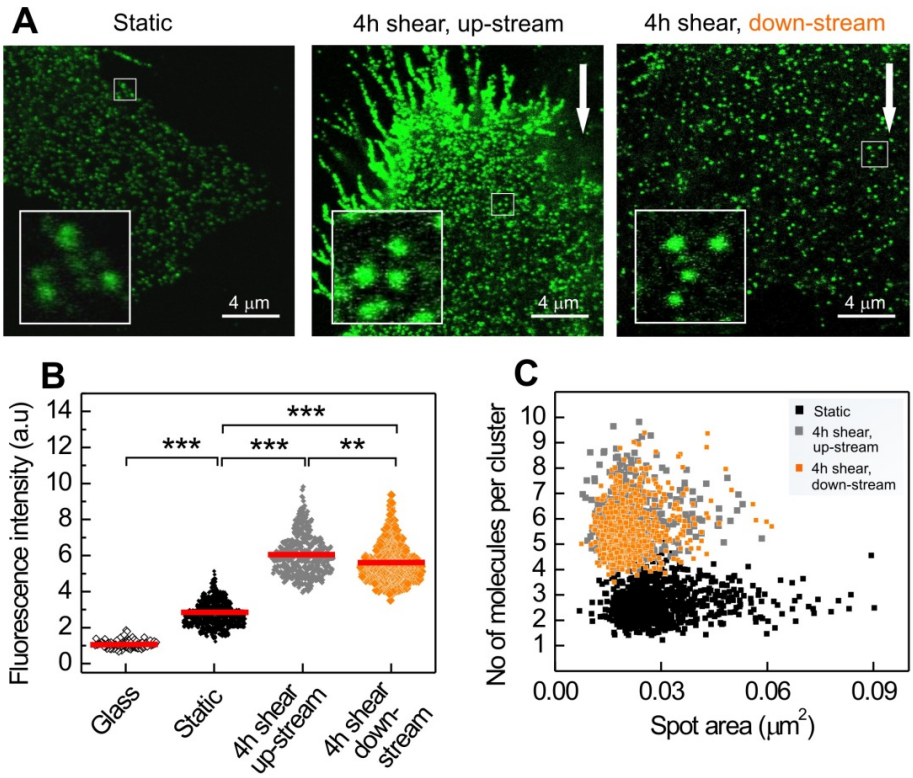


**Figure I.3 Effect of shear flow on ICAM-1 nanoclustering on TNF-α stimulated ECs. (A)** Representative STED images of ICAM-1 at the membrane of ECs in static conditions and after 4 hours of shear flow exposure. (*Insets*) Magnified views of individual ICAM-1 fluorescent spots. Arrows indicate the direction of shear flow. The spatial resolution is ~100nm **(B)** Normalized intensity per spot and **(C)** density distribution (#molecules/spot area) of ICAM-1 under static and shear conditions, as extracted from the analysis of the STED images. Data from individual Abs non- specifically attached to the glass are represented in (B). Intensity of ICAM-1 spots under the different conditions has been normalized to the mean intensity obtained on glass. In total, 10-15 individual ECs from two separate experiments were analysed per condition.

areas upstream of the 4h shear-stimulated cells that were excluded from our analysis due to an extremely high density of clusters. To quantify the number of ICAM-1 molecules contained in each cluster, we measured the fluorescence intensity of multiple spots on the membrane of different cells. For comparison, the intensity of individual antibodies that were found non-specifically absorbed on the glass and that represent the expected fluorescence intensity coming from single antibodies was also collected. In static conditions, we established that ICAM-1 is mainly organized in dimers and lower order multimers (Fig. I.3 B), in full agreement with previous reports[43–45].

Interestingly, a strong increase in the ICAM-1 cluster size was observed upon shear-stimulation. The larger clusters contain on average 5-6 molecules, but can be as large as 10 molecules (Fig. I.3 B). Since the actual cellular area that the larger clusters take up is unaffected by the flow (Fig. I.3 C), this means that ICAM-1 is more densely packed in shear-induced clusters. Even though many more clusters are found upstream on shear-stimulated cell as compared to downstream, the increase in cluster size is equally present. This indicates that the mechanism of ICAM-1 accumulation in larger clusters as a result of shear flow stimulation is a global phenomenon. Although it is well known that ICAM-1 organizes in microclusters upon engagement of integrins from the T-cell side[46–50], the nanoscale organization of ICAM-1 prior to T-cell engagement has not been reported yet (to the best of our knowledge). In summary, using super-resolution STED nanoscopy we showed that ICAM-1 molecules are part of the shear-sensitive EC machinery that rearrange in the response to continuous flow, forming nanoclusters on the EC surface that are highly localized on the upstream side of the ECs. As we further show in our submitted work using complementary techniques, this typical nanoscale organization has a major functional impact on the migratory behaviour of T lymphocytes bound to the endothelium during extravasation.[51]

**STORM – Stochastic optical reconstruction microscopy**

Together with Stefan Hell for his work on STED nanoscopy, Erik Betzig and William Moerner received the 2014 Nobel Prize in Chemistry for the development of super-resolved fluorescence microscopy. Their work paved the way for a second independent approach to break the diffraction limit collectively referred to as single molecule localization microscopy (SMLM)[52]. This approach relies on the notion that single fluorescent molecules can be detected[53] and localized[54] with very high precision by fitting their intensity profile to a Gaussian distribution. The precision with which the molecule can be localized solely depends on the amount of photons collected[53] so that for instance, for single molecules emitting typically $10^5$-to-$10^6$ photons before photodissociation, a localization precision in the order of few nanometres can be obtained, i.e., well beyond

the diffraction limit of light. However, this only applies when single molecules are well separated from each other ( > 250 nm) so that they can be distinguished and localized individually, which is naturally not the case in a fully labelled biological sample. Diluting the labelling density would give high localization precision for certain molecules in the sample, but would not generate a super-resolution image of the entire biological structure. To overcome this contradiction, SMLM relies on the on/off switching of fluorescent molecules, making only a small subset of them fluoresce at the time, allowing for their precise localization. Repeating this image acquisition thousands of times while randomly switching all the labelled molecules in the on-state ultimately provides the localization (*x* and *y* coordinates) of all fluorescent molecules in the sample. Based on all the localizations collected, a reconstructed super-resolution image can be generated with a resolution equal to the localization precision of typically around 20 nm (Fig. I.4) [55,56]. This can either be done by using photo- activatable (pa) fluorescent proteins such paGFP[55] or

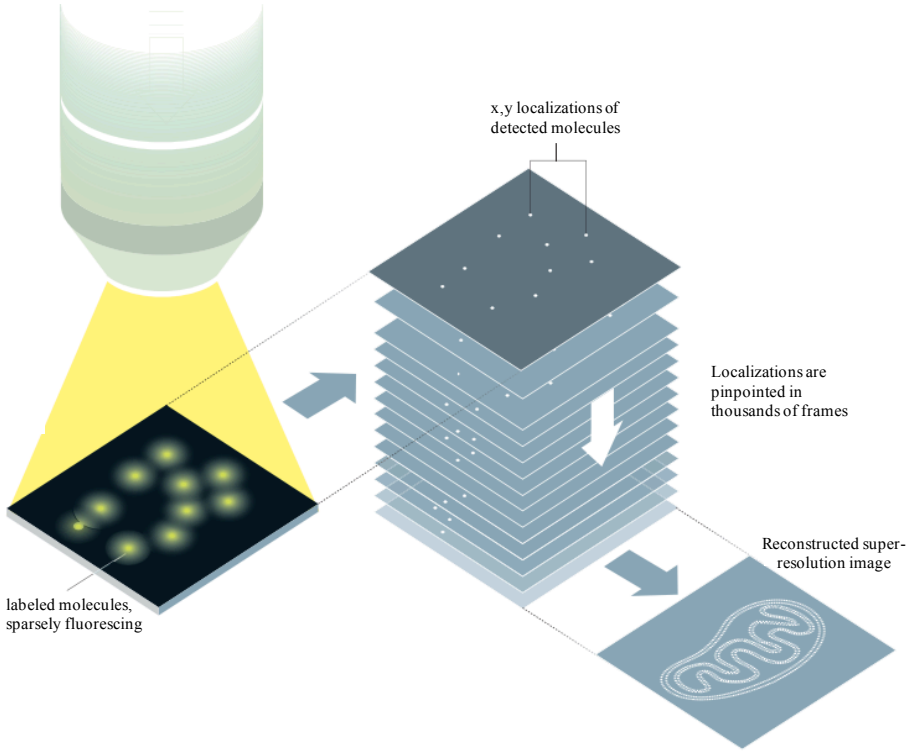


**Figure I.4: STORM principle explained.** STORM takes advantage of the on-off photoswitching properties of individual fluorophores to localize them with nanometric precision. The method is based on the repeated imaging of sparse stochastic subsets of fluorophores in the sample. The positions of active fluorophores are determined by finding their centroid positions by fitting to a Gaussian function, and then used to construct a super-resolution image of the labelled structure with an effective resolution around 20nm. Source of image: The royal Swedish academy of sciences.

photoswitchable organic dyes like Cy5 and AF647[56]. Both approaches were independently published in the same year, and are now referred to as PALM[55] (for fluorescent proteins) and STORM[56] (for organic dyes).

Now, 12 years since both landmark publications, countless papers have been published using either PALM or STORM to get nanometric information on a variety of biological subjects. Strategies have also been developed to image several colours at the same time[57–59], allowing for the characterization of different proteins within a complex relative to each other. The great gain in resolution obtained in these techniques however comes at the price of low throughput. Image acquisition takes a long time due to the thousands of frames needed to create a reconstructed image (typically 30-60 minutes), and post-image processing is far from trivial. This makes localization-based super-resolution imaging in my opinion most suited for fundamental structural biological questions at the nanoscale, where variations from cell to cell are minor. This poses a specific challenge in immunology, where researchers often have to deal with heterogeneous cell populations and different donors. Working with primary immune cells, STORM would be the technique of choice over PALM since it relies on antibody staining rather than transfection to express fluorescently labelled proteins. An elegant example of STORM imaging applied to structural questions in immunology is the nanoscale characterization of podosomes, an important adhesive structure in dendritic cells[60]. In addition, SMLM has been used to uncover the organization of different immunoproteins in lymphoid cell lines, including CD4[61], Lat[62] and Lck[63] on T cells and CD22 on B cells[64].

Another active field within STORM super-resolution is the structural organization of chromatin. Due to the extremely crowed environment in the nucleus and the nanometric size of the chromatin fibres, deciphering its structural organization within intact nuclei during interphase has long remained beyond reach. Several studies have now gained more insight in how our genetic material is stored by either looking at the DNA itself[65,66] or the histones around it[67,68]. All of these studies show a clear correlation between shape and functionality: transcriptionally active regions are less densely packed than inactive regions[66] and stem-cells exhibit a more open chromatin configuration than somatic cells[67]. This correlation paves the way for the use of structural STORM imaging to unravel functional changes in the genome at the single cell level. In Part II of this thesis we show a great example of how this strategy can be applied in nano-immunology. By quantifying the reconstructed super-resolution images of histone H2B labelling in the nuclei of human dendritic cells (DCs), we determined that the global chromatin density and therefore most likely the transcriptional activity changes along the differentiation of DCs. We also took advantage of dual-colour STORM imaging to characterize the spatial distribution of the immunoreceptor MerTK relative to the chromatin, in order to unravel its nuclear function.

In a different example described below, STORM super-resolution imaging has been used to quantify the impact of silver nanoclusters on chromatin compaction, targeted to increase the therapeutic impact of DNA-binding cytotoxic drugs. Even though in this case there is no direct connection to immunology, this work demonstrates the power of single molecule localization microscopy to reveal nanoscale re-organization of chromatin structure at the single cell level.

*Silver atomic quantum clusters of three atoms for cancer therapy: targeting chromatin compaction to increase the therapeutic index of chemotherapy*

DNA-binding cytotoxic drugs are the first choice in the treatment of many cancers. A major factor in the resistance of chemotherapy is that an insufficient amount of drug may reach the DNA, and chromatin is a major barrier that limits accessibility to DNA. Up to now, largely due to the lack of agents that can act on chromatin without other coupled effects, the importance of chromatin compaction affecting the action of chemotherapeutic DNA binding drugs could not be assessed. Using uncharged Ag clusters of only three atoms (named here Ag3-AQCs), our work provides evidence of the significance of targeting chromatin compaction to increase the therapeutic index of chemotherapy. To directly visualize the increased chromatin accessibility upon treatment with the $Ag_3$-AQCs, we performed super-resolution STORM microscopy on the nuclei of A549 proliferating cells. We visualized the newly replicated DNA labelled with EdU-AF647 (Fig. I.5 A) in the presence and absence of $Ag_3$-AQCs, as well as in the presence of free silver cations ($AgNO_3$) (Fig. I.5 B-D). The STORM images show a striking change of chromatin compaction upon the addition of the nanoparticles. Whereas in untreated cells the chromatin is contained in highly compact regions (magenta spots) (Fig. I.5 B), addition of the nanoparticles leads to a massive de-compaction of these regions (Fig. I.5 C). Quantification of STORM images on multiple cells shows that the chromatin occupies a larger percentage of the nuclear area (Fig. I.5 E) and that chromatin density decreases as a result of the nanoparticle treatment (Fig. I.5 F), consistent with chromatin de-compaction. These differences were specific to nanoparticle treatment, since silver cations did not affect chromatin compaction (Fig. I.5 D-F). These results directly demonstrate the increased accessibility of the chromatin leading to the increased therapeutic index of DNA-binding drugs, and also show that this effect is selectively induced by nanoparticles, and not by the presence of free silver cations in the media. *In vivo* experiments shown in our published work further demonstrate that increasing chromatin accessibility using silver nanoclusters augments the tumour-reducing effect of chemotherapy.[69]

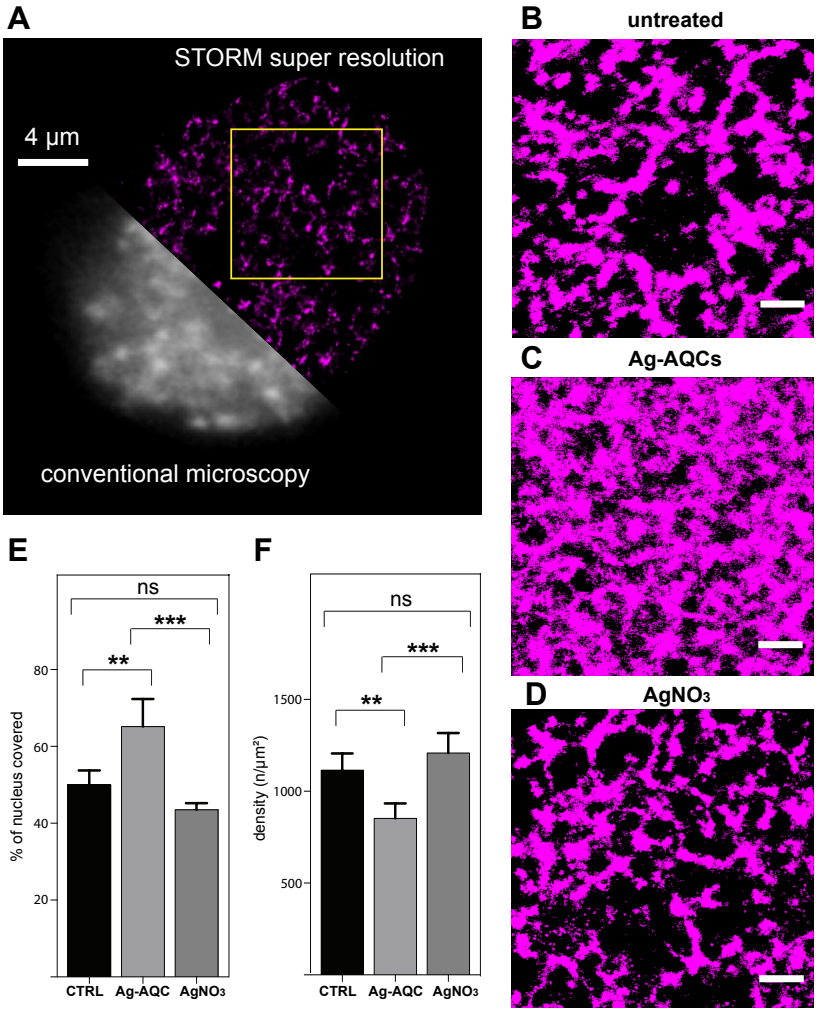


**Figure I.5. Direct visualization of chromatin accessibility using STORM super resolution microscopy**. The chromatin was labelled by allowing the incorporation of fluorescent EdU for two hours under different treatment conditions, and subsequently imaged using a commercial STORM system from Nikon. (**A**). Representative image of a nucleus containing fluorescent EdU, imaged using both conventional microscopy and STORM super resolution. The yellow square represents the size and typical location of the zoom-in images depicted in B-D. (**B-D**). Representative reconstructed STORM images of chromatin in cells in untreated (CTRL) conditions (**B**), after treatment with silver nanoparticles (**C**) and after treatment with free silver cations (**D**). Magenta spots represent single x-y localizations, while dark areas correspond to regions devoid of chromatin. All images are 50 $\mu m^2$ in size (typically representing about 1/3 of the nucleus as shown by the yellow square in **A**, and contain the same number of localizations allowing for reliable visual determination of differences in chromatin accessibility. Scale bars are 2 µm. (**E**) Quantification of the percentage of nuclear area covered by chromatin (percentage of non-zero pixels calculated in ImageJ). The number of localizations was kept constant across all images. (**F**) Quantification of the local chromatin density (number of localizations per covered area in E).

# I.3 Single-molecule dynamic approaches

**SPT - Single particle tracking**

At the basis of the lateral organization of immunoreceptors on the membrane lays their dynamic behaviour. This mechanism is shaping the nanolandscape of the plasma membrane and allows for rearrangements of receptors upon chemical stimuli as well as upon ligand binding. The study into the dynamic behaviour of immunoreceptors is therefore an active field of research. The above mentioned super-resolution techniques gain tremendously in lateral resolution, but lack however temporal resolution. STED nanoscopy is a scanning technique with a maximal temporal resolution of seconds, and due to its high laser power it is not very suited for repeated imaging on living cells. STORM super-resolution microscopy is inherently slow because of the thousands of frames that need to be acquired to obtain one single reconstructed image. Single Particle Tracking (SPT) provides an alternative method with millisecond temporal resolution and single molecule sensitivity[70–73]. Analogous to single molecule localization microscopy, the position of individual fluorescent probes that are well apart from each other is determined with nanometric precision in SPT. However, in this case the separation of the individual molecules comes from sub-labelling conditions, allowing one to track only a small percentage of receptors across the membrane. Unlike when looking for spatial information on a biological structure, sub-labelling conditions are no limitation in understanding the typical dynamic behaviour of a certain membrane protein. High frame-rate movies of a subset of fluorescently labelled receptors can thus be acquired over an extended period of time. Post-processing of the recorded movies entails pinpointing the position of all proteins in all frames, and the adequate connection of the recorded localizations of the same molecules over time, thereby defining its temporal trajectory (Figure I.6 A)[73]. The trajectories of many proteins on different regions of a cell and for different cells are ultimately used to derive the mobility behaviour of the receptor (Figure I.6 B-C).

The choice of the fluorescent label to track in SPT in very important. Brightness and photostability are key characteristics to take into account. The brighter the probe, the faster one acquires enough photons to pinpoint its location with high-precision and thus, higher frame-rates can be used. This leads to a better temporal resolution allowing the detection of important mobility characteristics of the receptor at short time-scales. On the other hand, a very photostable fluorescent probe facilitates the recording of longer movies, providing insight into the dynamic behaviour of a protein at longer time-scales and being more sensitive to changes in mobility over time. Ultimately, the photon budget of a fluo-

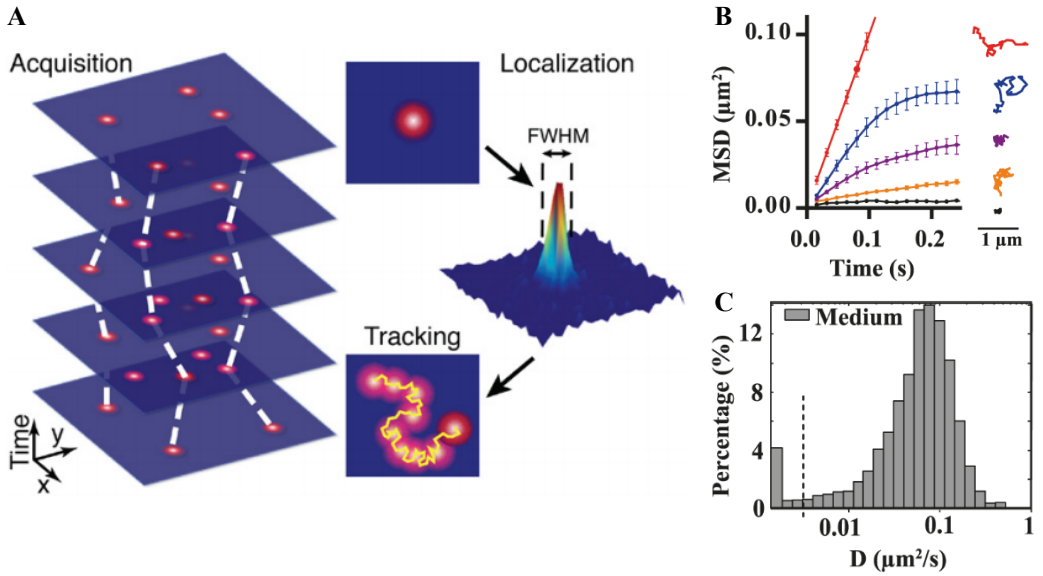


**Figure I.6 Single Particle Tracking principle explained.** (**A**) Schematic representation of SPT. In the acquisition step, a series of images is taken over time containing a sparse number of labelled molecules (red spots). Movies are typically hundreds to a few thousand frames long, recorded at a high frame-rate with a fast camera. In the localization step, the fluorescence image at a given time is analysed to retrieve the positions of the particles, analogous to SMLM. After repeating the localization step on a time series of images, the positions are linked to generate trajectories that track the motion of the particle[73]. (**B**) Mean square displacement plots extracted from 5 distinct trajectories ranging from immobile (dark blue) to fully mobile (red). The MSD represents the average area explored by a molecule from one frame to the next, and can be used to determine the diffusion coefficient as well as the mode of mobility (confined, free, directed). (**C**) Histogram of the instantaneous diffusion coefficient (D) of all the trajectories recorded in a certain condition, together making up the mobility profile of a protein in that condition. D is extracted from linearly fitting the 2$^{nd}$ to 4$^{th}$ point in the MSD plot. The vertical dotted line divides the immobile from the mobile population of receptors.

rescent probe is fixed and finite, and finding the right balance between the amount of photons collected per frame and the total amount of frames recorded is key. In the example below, we typically collected movies of 1000 frames at 60 Hz. Commonly used fluorescent probes, conjugated to an antibody against the protein of interest, are either organic photostable dyes such as ATTO647N[74,75] or quantum dots (QDs)[22,23,76,77]. QDs dots are extremely bright and photostable, and therefore ideal for recording long trajectories with a high frame-rate, containing more dynamic information. However, compared to organic dyes, QDs are very large, and therefore more likely to alter protein mobility by its presence. Especially for the tracking of membrane receptors on the basal membrane or the tracking of intracellular proteins where mobility interference is more of

a risk, organic dyes would be the probe of choice. In the example showed below we focused on the apical membrane of T-cells, and thus used QDs for their superior photophysical properties.

Typical parameters to report on the dynamic behaviour of a protein are the mean square displacement (MSD) and the diffusion coefficient (D). Both parameters can be extracted from the reconstructed trajectories. The MSD represents the average (of the entire trajectory) area explored by a mobile probe between one frame and the next. Figure I.6 B represents the MSD of different trajectories with a more (red) and less (dark blue) dynamic profile. Apart from whether the molecule is highly mobile or not, the MSD plot also contains information about the type of mobility. A linear MSD curve points to free mobility (red, yellow, dark blue), while a molecule with an MSD plot exhibiting a plateau at long times indicates confined motion (light blue, purple)[70]. To describe the degree of mobility of a molecule further on, the instantaneous diffusion coefficient is often used. This value comes from a linear fit through the 2$^{nd}$ to the 4$^{th}$ point of the MSD plot. The instantaneous diffusion coefficient is a good parameter to faithfully compare mobility across conditions/different proteins, since it is independent of the mode of mobility at long times (free, confined, directed). Plotting the $D_{2\text{-}4}$ of all trajectories recorded in a histogram (Figure I.6 C) finally gives a mobility profile of the protein of interest at short times. The diffusion coefficient obtained from fixed, non-mobile molecules stuck to the glass coverslip provides the cut-off value (dotted line in Fig. I.6 C) to discriminate between the mobile and immobile populations. Simply depicting the percentage of immobile molecules in different conditions is, in addition to the MSD and the $D_{2\text{-}4}$, also a well-established and straight-forward way to report on the degree of mobility of a certain protein.

In the following example, we used STP approaches to inquire on the mobility of the integrin receptor Very Late Antigen-4 (VLA-4) on the membrane of T-cells. The effect of both chemokine stimulation and ligand binding on the dynamics of VLA-4 is determined by comparing the mobility profile of the receptor across conditions.

*Lateral mobility and nanoscale spatial arrangement of chemokine-activated α4β1 integrins on T-cells*

Integrins are heterodimeric cell membrane adhesion receptors composed of non-covalently-associated α and β subunits which mediate cell-cell and cell-extracellular matrix adhesion[78]. In particular, the α4β1 (VLA-4) and αLβ2 (LFA-1) integrins are key players for T lymphocyte trafficking from blood circulation to lymphoid tissues and to

sites of injury and infection[78–80]. Their adhesiveness is rapidly and transiently activated by chemokines[79,80], allowing highly dynamic T cell interactions with the endothelium that facilitates crawling and diapedesis. The main binding partner of LFA-1 is ICAM-1[78], and the most important ligand for VLA-4 is VCAM-1[78].

A central question regarding integrin function on lymphocytes is how the lateral organization and mobility of α4β1 and αLβ2 influence their activation and adhesiveness after the contact with chemokines and/or ligands. Addressing this question is important in order to improve our understanding on how these integrins spatially regulate their affinity and avidity, and would ultimately allow interference in this process. Earlier reports on LFA-1 showed that its activation by extracellular cations or chemokine stimulation increases the percentage of immobile αLβ2 nanoclusters in dendritic cells, indicating that αLβ2 immobilization correlates with integrin activation[78]. Along the same lines, we previously showed that LFA-1 mobility is lost during DC differentiation[74], a process in which the same receptor also loses its ligand binding capacity at the same time[78]. In addition, we showed that reactivating LFA-1 by chemokine stimulation[40,41] also directly impacts on the mobility of the receptor[74]. For αLβ2 a strong correlation between activation and mobility has thus been established.

Little is known however about the mobility of α4β1 integrins on lymphocytes. In this work, we applied single-molecule approaches to study the potential lateral mobility alterations of α4β1 in response to chemokine stimulation. We showed that in analogy with LFA-1, the mobility of VLA-1 is transiently reduced upon CXCL12 treatment. The strongest immobilization is observed within the first 5 minutes after chemokine stimulation while mobility recovers again between 5 and 10 minutes (Figure I.7 A). We were able to correlate this reduced mobility to increased activity of the receptor by quantifying the amount of VLA-4 in an active confirmation (HUTS 21 antibody binding, Figure I.7 B). In addition, reduced mobility and integrin activation correlate with the binding of Talin-1 to VLA-4 (Figure I.7 C). Both conformational changes and Talin-1 binding are as transient as the observed mobility changes, further strengthening the correlation between all the three processes. Apart from being highly transient, the effect of CXCL12 on VLA-4 mobility and activation is also rather modest. This effect is however enormously potentiated when CXCL12 is administered in combination with ligand VCAM-1 (Figure I.7 A for mobility and B for activation). This is consistent with the role of ligands in stabilizing the active form of integrins brought about by chemokine-induced transient stimulation[40]. The overall conclusions of our work are based both on the well-accepted role that Talin plays in the transmission of inside-out signalling induced by

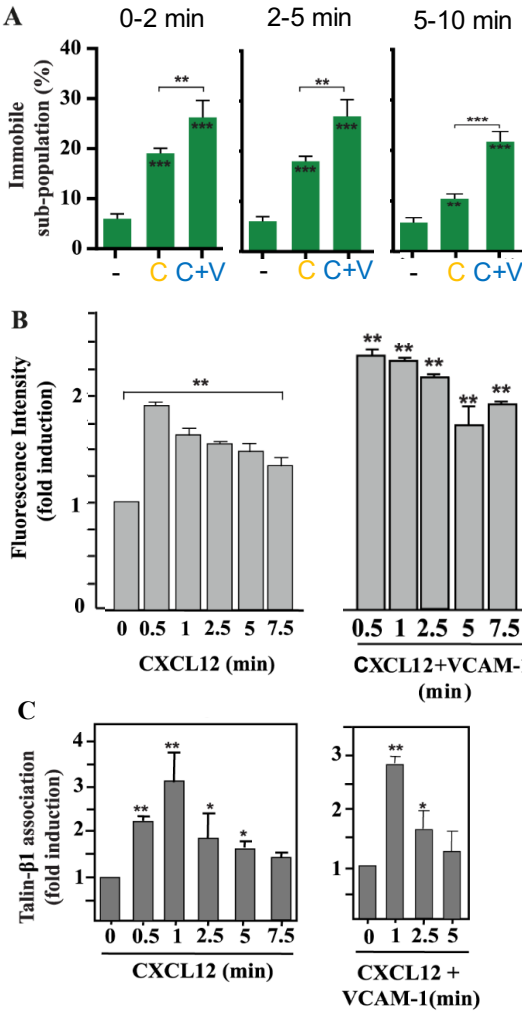


**Figure I.7 The effect of CXCL12 and ligand stimulation on VLA-4 mobility and activity. (A)** Percentage of immobile VLA-4 molecules in different conditions over time on Molt-4 T cells. VLA-4 mobility was measured in control conditions (-), with the addition of chemokine CXCL12 (C) and with the addition of both CXCL12 and ligand VCAM-1 (C+V). The immobile fraction was extracted from the $D_{2\text{-}4}$ distribution using a cut-off value of $D=0.0025\mu m^2/s$. (**B**) Molt-4 cells were exposed for the indicated times to CXCL12 alone or CXCL12+VCAM-1 and subjected to flow cytometry with the HUTS-21 anti-β1 antibody that only labels VLA-4 in an active conformation (N=3). Mean fluorescence intensity at different time points is depicted. (**C**) Cells were exposed to CXCL12 alone or CXCL12+VCAM-1 for the indicated times, and subsequently subjected to immunoprecipitation with the TS2/16 anti-β1 antibody that binds VLA-4 regardless of its conformation. This was then followed by immunoblotting with antibodies to Talin-1. The densitometric analyses of gel bands from the immunoprecipitations displaying the mean ±SD of four independent experiments are shown, indicating the relative amount of Talin-1 bound to VLA-4 in each condition.

chemokines for the generation of active α4β1 and αLβ2 integrins[81–83], and on our present results achieved using a combination of different techniques to link integrin activation and integrin immobilization. Thus, our data reveals a direct correlation between rapid and transient α4β1 immobilization via Talin association with β1 and conformational changes, which constitute clear indications of integrin activation. Talin comes into play by anchoring the activated integrin to the actin cytoskeleton, favouring receptor immobilization. In summary, our data indicate that fine-tuning and tight regulation of α4β1 immobilization and spatial arrangement on the cell surface, are crucial processes that modulate the integrin adhesiveness[84].

**FCS - Fluorescence correlation spectroscopy**

Fluorescence correlation spectroscopy (FCS) is an alternative technique to SPT to record the dynamic behaviour of biomolecules with a higher temporal resolution. This approach relies on recording the fluctuation in the fluorescence intensity over time within a confocal excitation volume (Figure I.8 A).[85] When applied to imaging a fluorescently labelled biomolecule on the plasma membrane, the intensity fluctuations will come from fluorescently labelled molecules moving in and out of the excitation area. At a specific moment in time, the amount of fluorescent molecules within the area will determine the intensity measured for that time point. Analysing the fluctuations of the fluorescence intensity over time (Figure I.8 B) provides information on the diffusive behaviour and the concentration of the molecule of interest.[86] This analysis is done by using an autocorrelation function (ACF), which consists of correlating a signal with a delayed copy of itself as a function of the delay time. This allows for the identification of repeating or period patterns within the signal. Typical ACF correlation plots display the probability (on the vertical axis) that a certain fluorescence molecule that was inside the excitation area at a specific time, will still be there after a given lag time (on the horizontal axis) (Figure I.8 C).[86] From the ACF curves, one can extract the characteristic diffusion time of the molecule of interest ($\tau_d$) by determining the lag time at half the amplitude. This diffusion time can then be used to calculate the diffusion coefficient. In addition, the amplitude of the ACF function at zero time lag is inversely proportional to the number of molecules traversing the illumination volume during the measurement (Figure I.8 C).

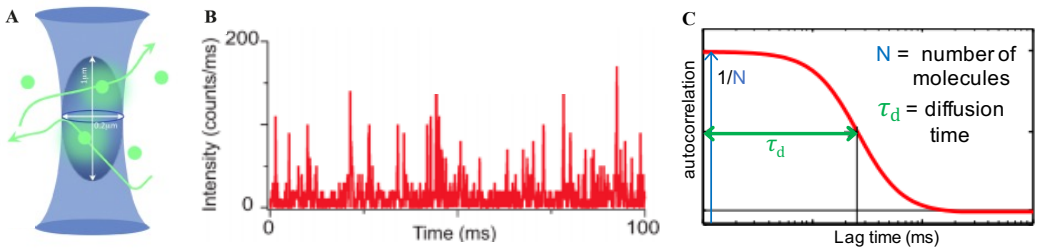


**Figure I.8: FCS explained.** (**A**) Schematic representation of the excitation volume for diffraction limited FCS. Fluorescently labelled molecules are diffusing in and out of the excitation volume in a characteristic fashion[87]. (**B**) Representative example of typical raw FCS measurements. The fluctuation in fluorescence intensity is recorded over time in a certain excitation volume. (**C**) Generalized example of an autocorrelation curve plotting the probability (vertical axis) that a certain fluorescent molecule remains inside the excitation volume for time lag x. The typical diffusion time (lag time at half the amplitude) and the number of molecules (1/(amplitude at zero lag time)) in the excitation volume during the measurement can be extracted from this correlation.

From here it also follows that the FCS technique works better at highly diluted concentrations so that the amplitude of the ACF is large and both the number of molecules and diffusion times can be estimated with higher precision.

In terms of temporal resolution, FCS is superior to SPT. This is because the temporal resolution of SPT is ultimately limited by the speed of the camera used (millisecond range). On the other hand, FCS has increased temporal resolution since it relies on single photon count detection using an APD (avalanche photodiode), which can even reach sub-micron second temporal resolution. Nevertheless, in both techniques, the practical temporal resolution is given by the number of photons being collected by the molecule under study. Since membrane lipids diffuse much faster that transmembrane receptors, FCS in membrane biology has been mostly used to record the mobility of lipids or lipid anchored proteins.

Standard FCS however lacks greatly in spatial resolution. The excitation area is defined by the diffraction limit, which is very large compared to single membrane proteins or lipids. For molecules diffusing in a random fashion, this illumination volume is not a limitation as long as the labelling is sufficiently diluted to allow for significant fluctuations. The larger the illumination volume, the longer it will take for a molecule to traverse the illumination volume, but its dynamic behaviour can be retrieved accurately taking both parameters into account. However, for molecules (lipids or proteins) exhibiting transient interactions with other molecules forming dynamic nanoclusters and/or with the membrane surrounding, their diffusion behaviour will significantly deviate from random. These interactions occurring at the nanometre scale would be reflected as an anomalous diffusion. Unfortunately, this anomalous behaviour will be averaged out with the diffraction-limited volume used for conventional FCS. In order to be more sensitive to transient interactions and anomalous diffusion at the nanoscale, FCS has been combined with several techniques that break the diffraction limit. A successful example is STED-FCS[88,89], where a confined excitation volume is created by using stimulated emission, a technique discussed in Section I.2. Instead of using the confined STED beam to image fixed cells using a scanning approach, the small excitation volume of STED is kept stationary and used to record fluorescence traces on live cells. Currently, it is possible with this technique to get dynamic measurements with a spatial resolution of around 30 nm[88]. The concerns related to the high depletion laser intensity already discussed in Section I,2 however persist and the application of STED-FCS in living cells remains highly challenging.

An alternative approach to bring FCS down to the nanoscale is by implementing this approach together with photonic nanoantennas. These metallic nanostructures increase the excitation light while simultaneously confine it down to the nanoscale in perfect analogy to what conventional antennas would do in the radiofrequency range[90,91]. While STED and STORM break the diffraction limit in the far-field, nanoantennas do so in the near-field, acting on evanescent waves instead of propagating waves. This implies that the antenna has to be brought in close contact with the fluorescent probe to be imaged (roughly closer than 10 nm). This can be done by using an antenna designed at the end of a near-field tip, and bringing this tip in close contact with the sample to be imaged using a near-field scanning optical microscope (NSOM)[92,93]. Our group has recently demonstrated that such an antenna design can provide dual colour and true spatial resolution of around 20 nm together with localization precision below 1 nm on immobilized fluorescent molecules[93]. However, getting the tip in close contact with a fluctuating living membrane without losing contact or damaging the cell is extremely challenging, making this approach less ideal for live cell studies. Moreover, these experiments have very low throughput since individual fluorescent trajectories are generated one by one, depending on the position where the nanoantenna is being placed with respect to the cell membrane. An alternative way to increase the measurement throughput without interference from the antenna tip is by using substrate antenna arrays. Our group has successfully combined these substrate antennas with FCS measurements at the nanoscale on molecules diffusing in solution[94]. The design has subsequently been improved in terms of planarity and biocompatibility, and was recently used to record the dynamic behaviour of fluorescent lipids diffusing in an artificially created lipid bilayer that was deposited directly onto the antenna substrate[95]. In the publication summarized below, we used these planar nanoantennas to study the mobility of different lipids in the membrane of living CHO cells.

This publication serves as a proof-of-concept that our approach is indeed compatible with live-cell imaging and therefore paves the way for using the same strategy to address currently open questions in membrane biology. Since this technique is mostly suited for the imaging of lipids rather than membrane proteins, the link to nano-immunology might not be immediately appreciated. However, it has become very clear from many studies over the last few decades that lipids play a major role in nano-landscaping the cell membrane, having a direct impact on the organization of transmembrane proteins[96,97] including immunoreceptors[98,99]. Studying lipid dynamics on immune cells is thus indeed very relevant in the understanding the behaviour of immune receptors.

*Planar optical nanoantennas resolve cholesterol-dependent nanoscale heterogeneities in the plasma membrane of living cells*

In this work, we combined FCS with planar optical nanogap antennas to investigate for the first time the nanoscopic organization of lipid rafts in the plasma membrane of living cells at a spatial resolution of 10 nm. The antenna design has been specifically developed for FCS with subdiffraction spatial resolution[94]. It combines a central nanogap dimer antenna to create the highly confined electromagnetic hotspot (with gap dimensions ~10 and 35 nm) surrounded by a rectangular cladding to prevent direct excitation of background molecules diffusing away from the central nanogap. By applying planarization, etch-back, and template stripping methods, we have improved our initial

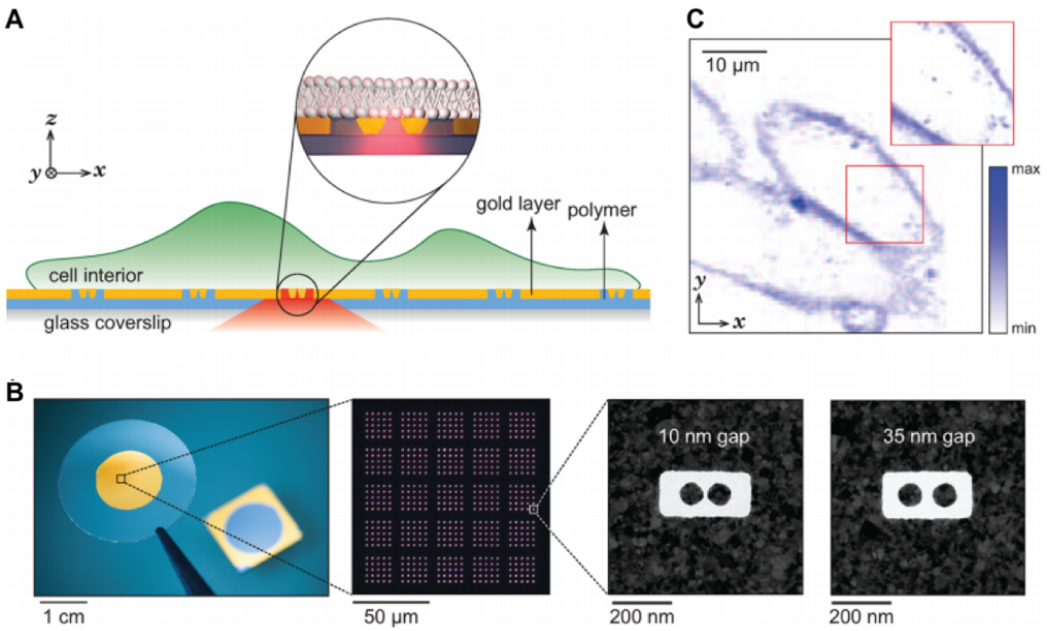


**Figure I.9**. **Planar gold nanoantenna arrays for probing single-molecule lipid dynamics in the plasma membrane of living cells**. (**A**) CHO cells are seeded onto a microscopic coverslip containing thousands of planar nanoantennas with 10 and 35 nm gap sizes. The inset shows the cross section of the antenna-in-box stripped and embedded into a polymer, bringing the region of maximum electromagnetic field intensity onto the surface in direct contact with the plasma membrane of living cells. (**B**) From left to right: macro-photograph of a coverslip with a stripped Au film with large-scale planar antenna arrays; dark field optical micrograph of a small portion of the antenna arrays showing here 625 antennas with 10 nm nominal gap size; transmission electron microscope (TEM) images of antennas with 10 and 35 nm gap sizes. (**C**) Confocal image of CHO cells after incorporating the fluorescent SM lipid analogue labelled with Atto647N. The cells were incubated on the nanoantennas at 37 °C for nearly 48 h prior to the experiments to allow them to freely grow and adhere onto the antenna platform. SM-Atto647N lipids were incorporated into the plasma membrane of the living cells just before the FCS measurements.

design to produce arrays of nanoantennas with controlled gap sizes, sharp edges, and planar hotspots facing the upper surface of the sample[100]. The planar antenna platform contains thousands of gold nanoantennas in different arrays on which a circular cell culture well is mounted for live CHO cell culturing. Figure I.9 depicts the strategy chosen for the fluorescence live cell experiment conducted on the nanogap antenna platform. A highly confined nanometric hotspot of illumination light is created on the surface of the nanogap region which is in direct contact with the adhered plasma membranes of living CHO cells. Importantly, the planarization strategy avoids possible curvature induced effects on the cell membrane and thus provides an ideal platform for live cell membrane research[95,101]. Using these planar nanoantennas with gap sizes down to 10 nm, we investigated the diffusion dynamics of phosphoethanolamine (PE) and sphingomyelin (SM) lipids on the plasma membrane of CHO cells. Unlike PE, SM is transiently trapped in cholesterol-enriched nanodomains of 10 nm diameter with short characteristic times around 100 μs. The removal of cholesterol led to the free diffusion of SM, consistent with the dispersion of nanodomains. Quantitative data on sphingolipids partitioning into nanodomains is crucial to understand the spatiotemporal heterogeneous organization of transient molecular complexes on the membrane of living cells at the nanoscale. Compared to earlier works using confocal FCS[102,103], nanoaperture FCS[104–106], or STED-FCS[88,89], our study is the first to breach into the sub-30 nm spatial scale on living cell membranes. The proposed technique is fully biocompatible and thus provides various opportunities for biophysics and live cell research to reveal details that remain hidden in confocal diffraction-limited measurements[107].

# I.4 Microfabrication tools to study protein interactions

### µCP - Microcontact printing

Microcontact printing (µCP) is a technique to directly stamp biomolecules onto a solid surface in almost any imaginable geometrical shape or pattern. Efficient ( > 99%) transfer from stamp to substrate rapidly occurs within a few seconds, without the loss of biological activity of the patterned molecules. PDMS is one of the materials of choice to fabricate the stamps. Its hydrophobicity ensures reversible absorbance of the 'ink' (molecules to be stamped) and its elastomeric properties facilitate close contact between stamp and surface. The PDMS stamps can be structured in almost any shape against a microfabricated silicon mold[108]. Figure I.10 A outlines the essential steps for the use of PDMS stamps to print proteins onto a glass substrate. The stamp is first incubated with a protein solution, which creates a monolayer of proteins on the surface of the stamp. After rinsing and drying, the proteins can be transferred onto the glass by stamping. Only the proteins at the interface of the stamp and the glass will be transferred during this process, resulting in a micropattern of protein on the substrate (Figure I.10 B and C)[109].

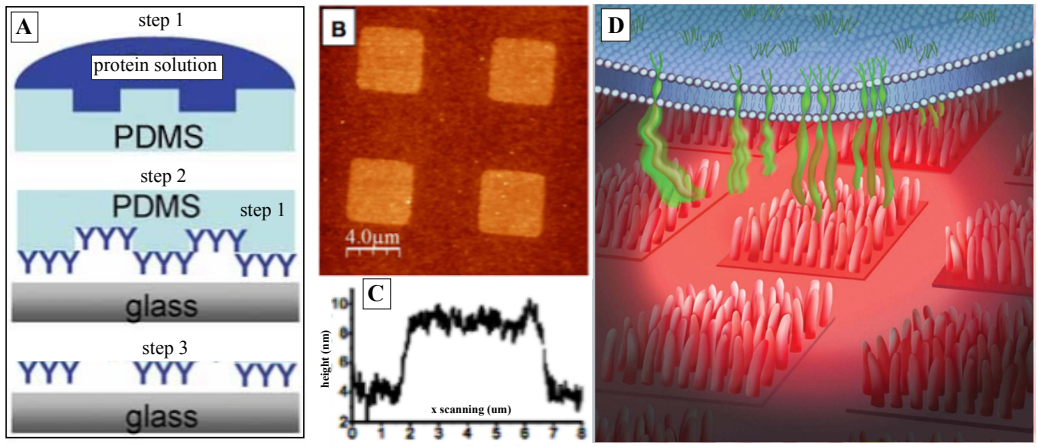


**Figure I.10: Microcontact printing explained.** (**A**) Schematic, step-wise representation of the use of PDMS micropatterns. In step 1, the PDMS mold is incubated with a protein solution containing the ligand or antibody of interest. In step 2, the PDMS covered by a monolayer of protein is used as a stamp to transfer the proteins onto the glass. Step 3 represents the result of the stamping, in which only the proteins at the PDMS-glass interface have transferred, resulting in a micropattern of proteins on the glass. (**B**) AFM inspection of the protein patterns on glass after step 3. Image is 20 x 20 $\mu m^2$ (256x256 pixels). (**C**) Line profile along the patterned protein area shown in B. The difference is height between positive and negative regions is ~ 5nm. (**D**) Artistic interpretation of the interaction between the proteins stamped on the glass in micropatterns and transmembrane receptors on the plasma membrane of a cell seeded on them. Figure is adapted from [109].

Important for the efficient transfer of proteins from the stamp onto the glass is the reversible absorbance of the ink to the PDMS. The proteins readily transfer from the PDMS onto the glass, but not the other way around. The mechanism for this one-way transfer is not completely understood, but it is clear that silanization of the glass prior to stamping, as well as a short time between drying the monolayer of proteins and using the stamp are both crucial factors[108].

Amongst many other applications, μCP is a great tool in studying immunoreceptors on the plasma membrane. By printing the ligand of a certain receptor on restricted areas of the glass, one can study for example the difference in dynamic behaviour of a particular receptor in the presence or absence of the ligand, all in a single SPT experiment[109]. One can even capture the change in behaviour within a single trajectory, which is extremely valuable in understanding the timing of events in receptor-ligand binding. Another example is the use of μCP to provide T cells with the counter molecules necessary to form an immunological synapse[110]. In this study, the migratory behaviour of T cells in the presence and absence of stimulation was recorded with the micropatterns allowing for a direct comparison between modes of migration[110]. Apart from studying dynamics across different printed substrates, μCP can also be interesting in studying protein-protein interactions at the cell surface. By printing patterns of antibodies against a certain membrane protein on glass, the receptor of interest accumulates on to the patterns due to its initial dynamic behaviour and trapping at the antibody patterns. Analogous to the more traditional immunoprecipitation (IP), μCP allows one to investigate the presence of other potentially interesting proteins in the areas of accumulation, in order to reveal which proteins interact with the original receptor of interest. The advantage over an IP is that this approach has subcellular resolution, and requires a low number of cells per experiment, which is specifically advantageous when working with primary immune cells. In the example below, we used this approach to study the interaction between LFA-1 and actin-binding protein Talin-1 on monocytes and mature DCs. As an additional advantage, μCP also allowed us to discriminate between Talin interaction with both resting as well as ligand activated LFA-1.

*Priming by chemokines restricts lateral mobility of the adhesion receptor LFA-1 and restored adhesion to ICAM-1 nanoaggregates on human mature dendritic cells*

Leukocyte specific integrins are a subfamily of transmembrane receptors involved in adhesion and migration of white blood cells. These receptors allow leukocytes to act upon the detection of potential threats to the body by enabling rapid anchoring of leukocytes to

the inner wall of blood vessels (extravasation). This process is followed by leukocyte migration from the bloodstream to the site of inflammation. In a subsequent step of the immunological cascade, leukocytes stably adhere to other immune cells to communicate the detected threat (immunological synapse formation)[111–114]. Lymphocyte Function-associated Antigen-1 (LFA-1) is a member of the leukocyte specific integrin family, and is amongst others expressed on lymphocytes, monocytes, and dendritic cells[115]. The main binding partner of LFA-1 is ICAM-1, which is highly expressed on activated endothelial cells and Antigen Presenting Cells (APCs) such as DCs[116,117]. To successfully accomplish the different types of adhesion in extravasation, migration and immunological synapse formation, tight regulation of LFA-1 activity is crucial.

During differentiation of monocytes into DCs, LFA-1-mediated binding to ICAM-1 is lost while expression levels of the receptor remain constant[19,78]. Activating mature DCs (mDCs) with chemokine CCL21 increases the population of activated LFA-1 molecules with high affinity for its ligand[78]. CCL21 is a chemokine that regulates the homing of lymphocytes and DCs from distant sites to lymphoid tissues[118–120] via binding to its receptor CCR7[121,122]. It has been shown in lymphocytes that soluble CCL21 triggers the high-affinity conformation of LFA-1[40] and induces binding of LFA-1 to its ligand ICAM-1[41]. Considering that LFA-1 conformation state and lateral diffusion on the cell membrane are highly coupled[123,124], it is conceivable that potential changes on the mobility of the receptor on mDCs after CCL21 stimulation might contribute together with affinity to the regain of LFA-1 functionality. Here we have performed systematic SPT studies (a technique discussed above) to directly report on the lateral mobility of LFA-1 on both monocytes and mDCs[74]. We showed that LFA-1 exhibits higher mobility on resting mDCs compared to monocytes. CCL21 stimulation of the high affinity state of LFA-1 on mDCs led to a significant reduction of LFA-1 lateral mobility, with overall diffusion profiles that closely resemble those obtained on resting monocytes. In analogy to VLA-4 discussed earlier, the effect of CCL21 on LFA-1 mobility is extremely rapid and transient, with a peak activation within the first 2 minutes after chemokine addition and loss of activation already after 4 minutes. The addition of soluble ICAM-1 nano-aggregates to CCL21 primed mDCs further reduced LFA-1 mobility and stabilized this profile over a longer time[74].

Immobilization of LFA-1 upon priming and ligand binding most probably corresponds to anchoring of the receptor to the actin cytoskeleton. Talin1 is a cytoplasmic protein that mediates the link between LFA-1 and the cytoskeleton[125,126], and is known to contribute to integrin function regulation and activation[40,127–130]. We therefore sought to investigate

the role of Talin1 in monocytes vs resting mDCs, as well as of activated mDCs. We used μCP to create square patterns of either TS2/4 binding Abs against LFA-1 or ligand ICAM-1 on glass coverslips following an established procedure[109]. TS2/4 patterns recruit LFA-1 without further manipulation, while ICAM-1 patterns would, in analogy to our mobility experiments, specifically recruit primed LFA-1 and subsequently further activate the receptor. As a negative control, we also used square patterns of mouse IgG1 isotype control antibodies not specific for LFA-1. We then seeded the cells on the patterned surfaces and allowed them to firmly adhere. Talin1 was fluorescently labelled, and the accumulation of the fluorescent signal to the LFA-1 rich areas was imaged (Figure I.11 A-D). To give a more quantitative dimension to our data, we used the fluorescent images of Talin (green) and positively patterned areas (red) to determine the specific accumulation of Talin to the patterns. We first selected the cell area in both channels, and created from the red channel a mask of the pattern (positive=1, negative=0). We applied this mask to the green channel, and calculated the average intensity per area of the green Talin signal in each positive square. To define the degree of enhancement in each positive area, this local average was divided by the average green intensity per area of the entire negative part of the mask covering the cell. To avoid artefacts, we excluded the negative region just around (up to 10 pixels away) a positive region. As a cut-off value to determine specific accumulation of Talin1 to the patterns, we used an enhancement factor > 1.5 (Figure I.11 E and F), since 95% of the data for resting monocytes on control IgG1 patterns falls below this value.

In resting as well as CCL21 stimulated monocytes, a rather diffused distribution of Talin1 was observed (Figure I.11A), independently on whether monocytes were seeded on a pattern of IgG1, TS2/4 or ICAM-1 (Figure I.11 E). This indicates that, in our experimental conditions, Talin1 in monocytes does not preferentially localize to LFA-1, neither in resting state nor upon ligand binding. In marked contrast, Talin1 preferentially localized to LFA-1 rich regions on mDCs, even without activation of LFA-1 by chemokine or ligand binding (Figure I.11 B-D and F). Notice however that we already observe a basal level of Talin1 accumulation (non-pattern related) close to the substrate that is aspecific for LFA-1 (Figure I.11 B). This patchy Talin1 accumulation probably corresponds to the formation of podosomes by mDCs[131], an adhesive structure in which $\beta_1$ and $\beta_3$ integrins as well as a Talin1 are involved[60]. In resting mDCs where LFA-1 is specifically recruited to the TS2/4 positive squares (Figure I.11 C), Talin1 accumulation to the patterns was significantly higher than to control IgG1 patterns (Figure I.11 F). LFA-1 priming using CCL21 (cells seeded on TS2/4 patterns) does not significantly increase Talin-1 accumulation beyond that observed in the resting state (Figure I.11 F). The same holds

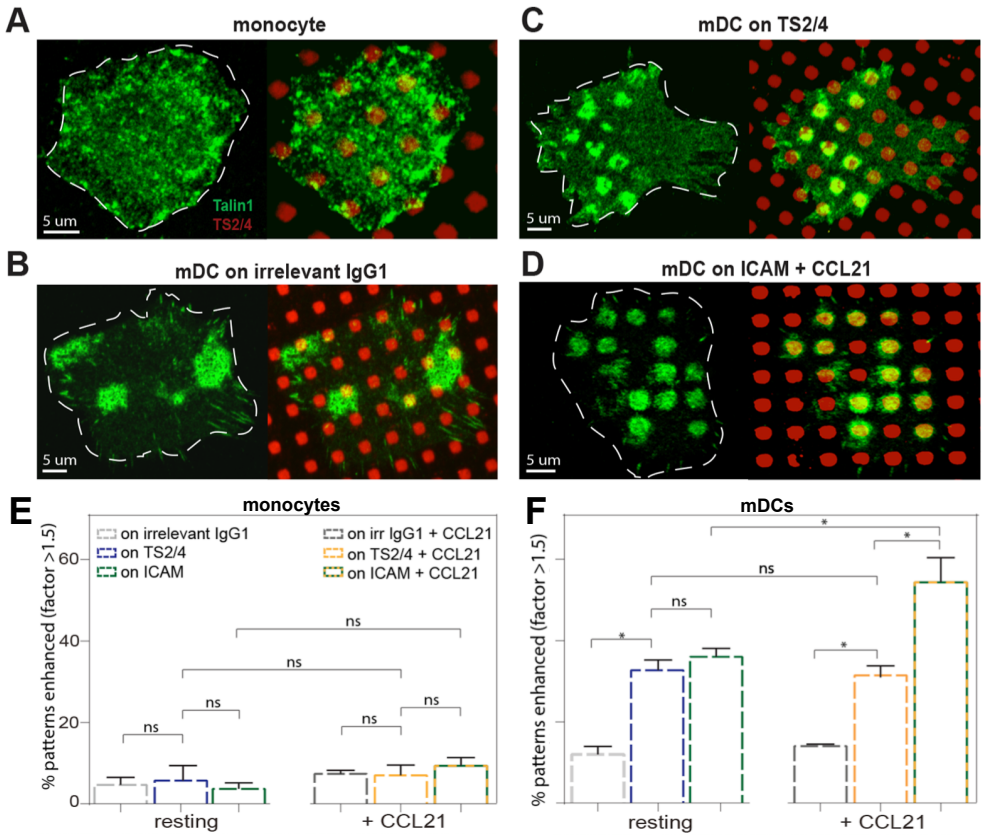


**Figure I.11: Localization of Talin1 to LFA-1 on monocytes and mDCs. (A-D)** Representative images of (**A**) a monocyte seeded on a TS2/4 pattern, (**B**) a resting mDC on irrelevant IgG1 pattern, (**C**) a resting mDC seeded on a TS2/4 pattern and (**D**) a CCL21 activated mDC seeded on a ICAM-1 pattern. Green corresponds to Talin1 and red to the location of IgG1, TS2/4 or ICAM-1 positive squares. Cells are delineated by white lines. (**E**) Percentage of positive squares per experiment (n = 3, each a different donor) that showed significantly enhanced Talin1 signal per condition in monocytes. An enhancement factor of ≥1.5 was considered significantly enhanced, since 95% of the control sample (monocytes on IgG1) showed an enhancement factor below this value. (**F**) Percentage of positive squares per experiment (n = 3, each a different donor) that showed significantly enhanced Talin1 signal per condition in mDCs. Around 60 cells of 3 different donors were analysed per condition. Monocytes contained 10 positive areas on average per cell, while mDCs contained around 50 positive areas.

for resting mDCs seeded on ICAM-1 patterns. These results thus show a basal association of LFA-1 with Talin1 already on resting mDCs, which is not affected by transient chemokine activation or ligand binding of LFA-1. On the other hand, the combination of both CCL21 priming and ligand binding highly increases Talin-1 accumulation to the

patterns (Figure I.11 D) up to a level where around 50% of the patterns shows significant enrichment of Talin1 (Figure 3.2 F). This increase is fully in line with the large reduction in mobility observed in the same conditions, and strengthens the hypothesis that immobilization of LFA-1 upon activation is the results of cytoskeleton anchoring mediated by Talin1.[74]

Knock-down and mutation of Talin1 has been shown to cause loss of ligand binding capacity of several $\beta_1$ and $\beta_3$ integrins[127,129], leading to a model explaining integrin activation as an event triggered by structural separation of the α and the β subunits due to Talin1 binding to the β-leg thereby inhibiting interaction with the α-leg[130]. In here we show that activation of LFA-1 by chemokine CCL21 does not increase Talin1 association to the integrin, unless ligand binding stabilizes this transient activation. This suggests that Talin1 recruitment to LFA-1 is a result of integrin activation rather than a trigger thereof. We further show preliminary evidence indicating that Talin1 might also play a different and more complex role in the regulation of $\beta_2$ integrins like LFA-1. We find that Talin1 already colocalizes with LFA-1 on mDCs in the resting state prior to integrin activation. This indicates that Talin1 in $\beta_2$ integrins is not only involved in maintaining LFA-1 in the active state, but also somehow in regulating resting, inactive LFA-1. Others have also observed association of Talin1 to LFA-1 on resting cells. Sampath *et al* showed that $\beta_2$-integrins on resting neutrophils, which belong together with DCs to the group of antigen presenting cells in which LFA-1 is inactive in resting state, co-immunoprecipitates with Talin1 (225 kDa)[132]. Upon activation however, $\beta_2$ co-immunoprecipitates with a smaller Talin1 (190 kDa) that only corresponds to the head domain. In addition, Kim *et al* showed that transfecting K562 cells with the Talin1 head domain exclusively indeed increases LFA-1 affinity and ligand binding[133]. Although in our experiments we could not discriminate between the full Talin1 or its head domain, it is clear that Talin1 does not only associate to LFA-1 upon activation. Instead, Talin could provide the receptor with the possibility of becoming activated through its cleavage, brought about by additional factors such as chemokines.

Overall, our results underscore three main features associated to LFA-1 activation and function. First, lateral mobility of the receptor is directly correlated with its activation state, with LFA-1 priming resulting in restricted lateral diffusion. Second, chemokines are required but not sufficient to maintain the high affinity state of the receptor, which is stabilized by multi-ligand binding. Lastly, our experiments using micropatterning show that a Talin1 is involved in regulating the functionality of LFA-1 not only upon activation, but already in the inactive state. This result suggests that instead of being an activating agent itself, Talin1 is more likely a protein providing LFA-1 with the possibility to become activated by additional factors such as chemokines.[74]

# I.5 References


1. Kindt TJ, Goldsby RA, Osborne BA, Kuby J. Kuby immunology. New York: W.H. Freeman; 2007.
2. Pockley AG, Foulds GA, Oughton JA, Kerkvliet NI, Multhoff G. Immune Cell Phenotyping Using Flow Cytometry. *Curr. Protoc. Toxicol.* 2015;66(1):18.8.1-18.8.34.
3. Craig FE, Foon KA. Flow cytometric immunophenotyping for hematologic neoplasms. *Blood*. 2008;111(8):3941–67.
4. Look AT, Roberson PK, Williams DL, et al. Prognostic importance of blast cell DNA content in childhood acute lymphoblastic leukemia. *Blood*. 1985;65(5):1079–86.
5. Bigley V, Barge D, Collin M. Dendritic cell analysis in primary immunodeficiency. *Curr. Opin. Allergy Clin. Immunol.* 2016;16(6):530–540.
6. Bacher P, Scheffold A. New technologies for monitoring human antigen-specific T cells and regulatory T cells by flow-cytometry. *Curr. Opin. Pharmacol.* 2015;23:17–24.
7. Lanier LL. Just the FACS. *J. Immunol.* 2014;193(5):2043–4.
8. Abbe E. Beiträge zur Theorie des Mikroskops und der mikroskopischen Wahrnehmung. *Arch. für Mikroskopische Anat.* 1873;9(1):413–418.
9. Saka SK, Honigmann A, Eggeling C, et al. Multi-protein assemblies underlie the mesoscale organization of the plasma membrane. *Nat. Commun.* 2014;5(1):4509.
10. Hell SW, Wichmann J. Breaking the diffraction resolution limit by stimulated emission: stimulated-emission-depletion fluorescence microscopy. *Opt. Lett.* 1994;19(11):.
11. Eggeling C. Super-resolution optical microscopy of lipid plasma membrane dynamics. *Essays Biochem.* 2015;57:69–80.
12. Rittweger E, Han KY, Irvine SE, Eggeling C, Hell SW. STED microscopy reveals crystal colour centres with nanometric resolution. *Nat. Photonics*. 2009;3(3):144–147.
13. Grotjohann T, Testa I, Leutenegger M, et al. Diffraction-unlimited all-optical imaging and writing with a photochromic GFP. *Nature*. 2011;478(7368):204–208.
14. Oracz J, Westphal V, Radzewicz C, Sahl SJ, Hell SW. Photobleaching in STED nanoscopy and its dependence on the photon flux applied for reversible silencing of the fluorophore. *Sci. Rep.* 2017;7(1):11354.
15. Li C, Liu S, Wang W, et al. Recent research on stimulated emission depletion microscopy for reducing photobleaching. *J. Microsc.* 2018;
16. Balzarotti F, Eilers Y, Gwosch KC, et al. Nanometer resolution imaging and tracking of fluorescent molecules with minimal photon fluxes. *Science (80-. ).* 2017;355(6325):606–612.
17. Wurm CA, Kolmakov K, Göttfert F, et al. Novel red fluorophores with superior performance in STED microscopy. *Opt. Nanoscopy*. 2012;1(1):7.
18. Garcia-Parajo MF, Cambi A, Torreno-Pina JA, Thompson N, Jacobson K. Nanoclustering as a dominant feature of plasma membrane organization. *J. Cell Sci.* 2014;127(23):4995–5005.
19. Cambi A, Joosten B, Koopman M, et al. Organization of the Integrin LFA-1 in Nanoclusters Regulates Its Activity. *Mol. Biol. Cell*. 2006;17(10):4270–4281.
20. Yang J, Reth M. Oligomeric organization of the B-cell antigen receptor on resting cells. *Nature*. 2010;467(7314):465–469.
21. Schamel WWA, Alarcón B. Organization of the resting TCR in nanoscale oligomers. *Immunol. Rev.* 2013;251(1):13–20.
22. Torreno-Pina JA, Castro BM, Manzo C, et al. Enhanced receptor-clathrin interactions induced by N-glycan-mediated membrane micropatterning. *Proc. Natl. Acad. Sci. U. S. A.* 2014;111(30):11037–42.
23. Torreno-Pina JA, Manzo C, Salio M, et al. The actin cytoskeleton modulates the activation of iNKT cells by segregating CD1d nanoclusters on antigen-presenting cells.

*Proc. Natl. Acad. Sci. U. S. A.* 2016;113(6):E772-81.
24. Kansas GS. Selectins and their ligands: current concepts and controversies. *Blood*. 1996;88(9):3259–87.
25. Campbell JJ, Hedrick J, Zlotnik A, et al. Chemokines and the arrest of lymphocytes rolling under flow conditions. *Science (80-. ).* 1998;279(5349):381–4.
26. Schenkel AR, Mamdouh Z, Muller WA. Locomotion of monocytes on endothelium is a critical step during extravasation. *Nat. Immunol.* 2004;5(4):393–400.
27. Dejana E. The transcellular railway: insights into leukocyte diapedesis. *Nat. Cell Biol.* 2006;8(2):105–7.
28. Ley K, Laudanna C, Cybulsky MI, Nourshargh S. Getting to the site of inflammation: the leukocyte adhesion cascade updated. *Nat. Rev. Immunol.* 2007;7(9):678–689.
29. Oppenheimer-Marks N, Davis LS, Bogue DT, Ramberg J, Lipsky PE. Differential utilization of ICAM-1 and VCAM-1 during the adhesion and transendothelial migration of human T lymphocytes. *J. Immunol.* 1991;147(9):2913–21.
30. Makgoba MW, Sanders ME, Ginther Luce GE, et al. ICAM-1 a ligand for LFA-1-dependent adhesion of B, T and myeloid cells. *Nature*. 1988;331(6151):86–8.
31. Nagel T, Resnick N, Atkinson WJ, Dewey CF, Gimbrone MA. Shear stress selectively upregulates intercellular adhesion molecule-1 expression in cultured human vascular endothelial cells. *J. Clin. Invest.* 1994;94(2):885–891.
32. Tsuboi H, Ando J, Korenaga R, Takada Y, Kamiya A. Flow stimulates ICAM-1 expression time and shear stress dependently in cultured human endothelial cells. *Biochem. Biophys. Res. Commun.* 1995;206(3):988–96.
33. Topper JN, Gimbrone MA. Blood flow and vascular gene expression: fluid shear stress as a modulator of endothelial phenotype. *Mol. Med. Today*. 1999;5(1):40–6.
34. Chien S, Li S, Shyy YJ. Effects of mechanical forces on signal transduction and gene expression in endothelial cells. *Hypertens. (Dallas, Tex. 1979)*. 1998;31(1 Pt 2):162–9.
35. Wojciak-Stothard B, Ridley AJ. Shear stress–induced endothelial cell polarization is mediated by Rho and Rac but not Cdc42 or PI 3-kinases. *J. Cell Biol.* 2003;161(2):429–439.
36. Davies PF, Robotewskyj A, Griem ML. Quantitative studies of endothelial cell adhesion. Directional remodeling of focal adhesion sites in response to flow forces. *J. Clin. Invest.* 1994;93(5):2031–8.
37. Butler PJ, Norwich G, Weinbaum S, Chien S. Shear stress induces a time- and position-dependent increase in endothelial cell membrane fluidity. *Am. J. Physiol. Cell Physiol.* 2001;280(4):C962-9.
38. Yamamoto K, Ando J. Endothelial cell and model membranes respond to shear stress by rapidly decreasing the order of their lipid phases. *J. Cell Sci.* 2013;126(Pt 5):1227–34.
39. Morigi M, Zoja C, Figliuzzi M, et al. Fluid shear stress modulates surface expression of adhesion molecules by endothelial cells. *Blood*. 1995;85(7):1696–703.
40. Shamri R, Grabovsky V, Gauguet J-M, et al. Lymphocyte arrest requires instantaneous induction of an extended LFA-1 conformation mediated by endothelium-bound chemokines. *Nat. Immunol.* 2005;6(5):497–506.
41. Constantin G, Majeed M, Giagulli C, et al. Chemokines trigger immediate beta2 integrin affinity and mobility changes: differential regulation and roles in lymphocyte arrest under flow. *Immunity*. 2000;13(6):759–69.
42. Cinamon G, Shinder V, Alon R. Shear forces promote lymphocyte migration across vascular endothelium bearing apical chemokines. *Nat. Immunol.* 2001;2(6):515–22.
43. Miller J, Knorr R, Ferrone M, et al. Intercellular adhesion molecule-1 dimerization and its consequences for adhesion mediated by lymphocyte function associated-1. *J. Exp. Med.* 1995;182(5):1231–41.
44. Bene L, Balázs M, Matkó J, et al. Lateral organization of the ICAM-1 molecule at the surface of human lymphoblasts: a possible model for its co-distribution with the IL-2

receptor, class I and class II HLA molecules. *Eur. J. Immunol.* 1994;24(9):2115–23.
45. Jun CD, Carman C V, Redick SD, et al. Ultrastructure and function of dimeric, soluble intercellular adhesion molecule-1 (ICAM-1). *J. Biol. Chem.* 2001;276(31):29019–27.
46. Yang L, Kowalski JR, Yacono P, et al. Endothelial cell cortactin coordinates intercellular adhesion molecule-1 clustering and actin cytoskeleton remodeling during polymorphonuclear leukocyte adhesion and transmigration. *J. Immunol.* 2006;177(9):6440–9.
47. Millán J, Hewlett L, Glyn M, et al. Lymphocyte transcellular migration occurs through recruitment of endothelial ICAM-1 to caveola- and F-actin-rich domains. *Nat. Cell Biol.* 2006;8(2):113–23.
48. Shaw SK, Ma S, Kim MB, et al. Coordinated redistribution of leukocyte LFA-1 and endothelial cell ICAM-1 accompany neutrophil transmigration. *J. Exp. Med.* 2004;200(12):1571–80.
49. Carman C V, Jun C-D, Salas A, Springer TA. Endothelial cells proactively form microvilli-like membrane projections upon intercellular adhesion molecule 1 engagement of leukocyte LFA-1. *J. Immunol.* 2003;171(11):6135–44.
50. Barreiro O, Yanez-Mo M, Serrador JM, et al. Dynamic interaction of VCAM-1 and ICAM-1 with moesin and ezrin in a novel endothelial docking structure for adherent leukocytes. *J. Cell Biol.* 2002;157(7):1233–45.
51. Piechocka IK, Sosa-Costa A, Mohan N, Borgman KJE, Keary S, Lakadamyali M, Manzo C G-PM. Shear flow driven actin reorganization promotes ICAM-1 nanoclustering on endothelial cells effecting T-cell migration. *Submitt. to J. Cell Sci.* .
52. Sauer M, Heilemann M. Single-Molecule Localization Microscopy in Eukaryotes. *Chem. Rev.* 2017;117(11):7478–7509.
53. Moerner WE, Kador L. Optical detection and spectroscopy of single molecules in a solid. *Phys. Rev. Lett.* 1989;62(21):2535–2538.
54. Thompson RE, Larson DR, Webb WW. Precise nanometer localization analysis for individual fluorescent probes. *Biophys. J.* 2002;82(5):2775–83.
55. Betzig E, Patterson GH, Sougrat R, et al. Imaging Intracellular Fluorescent Proteins at Nanometer Resolution. *Science (80-. ).* 2006;313(5793):1642–1645.
56. Rust MJ, Bates M, Zhuang X. Sub-diffraction-limit imaging by stochastic optical reconstruction microscopy (STORM). *Nat. Methods*. 2006;3(10):793–796.
57. Bates M, Huang B, Dempsey GT, Zhuang X. Multicolor super-resolution imaging with photo-switchable fluorescent probes. *Science*. 2007;317(5845):1749–1753.
58. Tam J, Cordier GA, Borbely JS, Sandoval Álvarez A, Lakadamyali M. Cross-talk-free multi-color STORM imaging using a single fluorophore. *PLoS One*. 2014;9(7):e101772.
59. Dempsey GT, Vaughan JC, Chen KH, Bates M, Zhuang X. Evaluation of fluorophores for optimal performance in localization-based super-resolution imaging. *Nat. Methods*. 2011;8(12):1027–1036.
60. van den Dries K, Schwartz SL, Byars J, et al. Dual-color superresolution microscopy reveals nanoscale organization of mechanosensory podosomes. *Mol. Biol. Cell*. 2013;24(13):2112–23.
61. Roh K-H, Lillemeier BF, Wang F, Davis MM. The coreceptor CD4 is expressed in distinct nanoclusters and does not colocalize with T-cell receptor and active protein tyrosine kinase p56lck. *Proc. Natl. Acad. Sci. U. S. A.* 2015;112(13):E1604-13.
62. Sherman E, Barr V, Manley S, et al. Article Functional Nanoscale Organization of Signaling Molecules Downstream of the T Cell Antigen Receptor. *Immunity*. 2011;35:705–720.
63. Rossy J, Owen DM, Williamson DJ, Yang Z, Gaus K. Conformational states of the kinase Lck regulate clustering in early T cell signaling. *Nat. Immunol.* 2013;14(1):82–89.
64. Gasparrini F, Feest C, Bruckbauer A, et al. Nanoscale organization and dynamics of the siglec CD22 cooperate with the cytoskeleton in restraining BCR signalling. *EMBO J.*

2016;35(3):258–80.
65. Zessin PJM, Finan K, Heilemann M. Super-resolution fluorescence imaging of chromosomal DNA. *J. Struct. Biol.* 2012;177(2):344–348.
66. Boettiger AN, Bintu B, Moffitt JR, et al. Super-resolution imaging reveals distinct chromatin folding for different epigenetic states. *Nature*. 2016;529(7586):418–22.
67. Ricci MA, Manzo C, Garcia-Parajo MF, Lakadamyali M, Cosma MP. Chromatin fibers are formed by heterogeneous groups of nucleosomes in vivo. *Cell*. 2015;160(6):1145–1158.
68. Lakadamyali M, Cosma MP. Advanced microscopy methods for visualizing chromatin structure. *FEBS Lett.* 2015;589(20):3023–3030.
69. Porto V, Borrajo E, Buceta D, et al. Silver Atomic Quantum Clusters of Three Atoms for Cancer Therapy: Targeting Chromatin Compaction to Increase the Therapeutic Index of Chemotherapy. *Adv. Mater.* 2018;1801317.
70. Kusumi A, Sako Y, Yamamoto M. Confined lateral diffusion of membrane receptors as studied by single particle tracking (nanovid microscopy). Effects of calcium-induced differentiation in cultured epithelial cells. *Biophys. J.* 1993;65(5):2021–40.
71. Alcor D, Gouzer G, Triller A. Single-particle tracking methods for the study of membrane receptors dynamics. *Eur. J. Neurosci.* 2009;30(6):987–997.
72. Cognet L, Lounis B, Choquet D. Tracking Receptors Using Individual Fluorescent and Nonfluorescent Nanolabels. *Cold Spring Harb. Protoc.* 2014;(2):207–13.
73. Manzo C, Garcia-Parajo MF. A review of progress in single particle tracking: from methods to biophysical insights. *Reports Prog. Phys.* 2015;78(12):124601.
74. Borgman KJE, Van Zanten TS, Manzo C, et al. Priming by chemokines restricts lateral mobility of the adhesion receptor LFA-1 and restores adhesion to ICAM-1 nano-aggregates on human mature dendritic cells. *PLoS One*. 2014;9(6):.
75. Bakker GJ, Eich C, Torreno-Pina JA, et al. Lateral mobility of individual integrin nanoclusters orchestrates the onset for leukocyte adhesion. *Proc. Natl. Acad. Sci. U. S. A.* 2012;109(13):4869–74.
76. Bannai H, Lévi S, Schweizer C, Dahan M, Triller A. Imaging the lateral diffusion of membrane molecules with quantum dots. *Nat. Protoc.* 2007;1(6):2628–2634.
77. Chang Y-P, Pinaud F, Antelman J, Weiss S. Tracking bio-molecules in live cells using quantum dots. *J. Biophotonics*. 2008;1(4):287–298.
78. Eich C, de Vries IJM, Linssen PC, et al. The lymphoid chemokine CCL21 triggers LFA-1 adhesive properties on human dendritic cells. *Immunol. Cell Biol.* 2011;89(3):458–465.
79. Hogg N, Henderson R, Leitinger B, et al. Mechanisms contributing to the activity of integrins on leukocytes. *Immunol. Rev.* 2002;186:164–71.
80. Oppenheimer-Marks N, Davis LS, Bogue DT, Ramberg J, Lipsky PE. Differential utilization of ICAM-1 and VCAM-1 during the adhesion and transendothelial migration of human T lymphocytes. *J. Immunol.* 1991;147(9):2913–21.
81. Lefort CT, Rossaint J, Moser M, et al. Distinct roles for talin-1 and kindlin-3 in LFA-1 extension and affinity regulation. *Blood*. 2012;119(18):4275–82.
82. García-Bernal D, Parmo-Cabañas M, Dios-Esponera A, et al. Chemokine-induced Zap70 kinase-mediated dissociation of the Vav1-talin complex activates alpha4beta1 integrin for T cell adhesion. *Immunity*. 2009;31(6):953–64.
83. Manevich E, Grabovsky V, Feigelson SW, Alon R. Talin 1 and paxillin facilitate distinct steps in rapid VLA-4-mediated adhesion strengthening to vascular cell adhesion molecule 1. *J. Biol. Chem.* 2007;282(35):25338–48.
84. Sosa-Costa A, Isern de Val S, Sevilla-Movilla S, et al. Lateral Mobility and Nanoscale Spatial Arrangement of Chemokine-activated α4β1 Integrins on T Cells. *J. Biol. Chem.* 2016;291(40):21053–21062.
85. Magde D, Elson E, Webb WW. Thermodynamic Fluctuations in a Reacting System—Measurement by Fluorescence Correlation Spectroscopy. *Phys. Rev. Lett.*

1972;29(11):705–708.
86. Schwille P, Korlach J, Webb WW. Fluorescence correlation spectroscopy with single-molecule sensitivity on cell and model membranes. *Cytometry*. 1999;36(3):176–182.
87. Briddon SJ, Kilpatrick LE, Hill SJ. Studying GPCR Pharmacology in Membrane Microdomains: Fluorescence Correlation Spectroscopy Comes of Age. *Trends Pharmacol. Sci.* 2018;39(2):158–174.
88. Vicidomini G, Ta H, Honigmann A, et al. STED-FLCS: An Advanced Tool to Reveal Spatiotemporal Heterogeneity of Molecular Membrane Dynamics. *Nano Lett.* 2015;15(9):5912–8.
89. Eggeling C, Ringemann C, Medda R, et al. Direct observation of the nanoscale dynamics of membrane lipids in a living cell. *Nature*. 2009;457(7233):1159–62.
90. Novotny L, van Hulst N. Antennas for light. *Nat. Photonics*. 2011;5(2):83–90.
91. Garcia-Parajo MF. Optical antennas focus in on biology. *Nat. Photonics*. 2008;2(4):201–203.
92. Betzig E, Trautman JK. Near-field optics: Microscopy, spectroscopy, and surface modification beyond the diffraction limit. *Science (80-. ).* 1992;257(5067):189–195.
93. Mivelle M, van Zanten TS, Garcia-Parajo MF. Hybrid Photonic Antennas for Subnanometer Multicolor Localization and Nanoimaging of Single Molecules. *Nano Lett.* 2014;14(8):4895–4900.
94. Punj D, Mivelle M, Moparthi SB, et al. A plasmonic 'antenna-in-box' platform for enhanced single-molecule analysis at micromolar concentrations. *Nat. Nanotechnol.* 2013;8(7):512–516.
95. Winkler PM, Regmi R, Flauraud V, et al. Transient Nanoscopic Phase Separation in Biological Lipid Membranes Resolved by Planar Plasmonic Antennas. *ACS Nano*. 2017;11(7):7241–7250.
96. Lingwood D, Simons K. Lipid Rafts As a Membrane-Organizing Principle. *Science (80-. ).* 2010;327(5961):46–50.
97. Bollinger CR, Teichgräber V, Gulbins E. Ceramide-enriched membrane domains. *Biochim. Biophys. Acta - Mol. Cell Res.* 2005;1746(3):284–294.
98. van Zanten TS, Cambi A, Koopman M, et al. Hotspots of GPI-anchored proteins and integrin nanoclusters function as nucleation sites for cell adhesion. *Proc. Natl. Acad. Sci. U. S. A.* 2009;106(44):18557–62.
99. Eich C, Manzo C, Keijzer S de, et al. Changes in membrane sphingolipid composition modulate dynamics and adhesion of integrin nanoclusters. *Sci. Rep.* 2016;6(1):20693.
100. Flauraud V, Regmi R, Winkler PM, et al. In-Plane Plasmonic Antenna Arrays with Surface Nanogaps for Giant Fluorescence Enhancement. *Nano Lett.* 2017;17(3):1703–1710.
101. Kelly C V, Baird BA, Craighead HG. An array of planar apertures for near-field fluorescence correlation spectroscopy. *Biophys. J.* 2011;100(7):L34-6.
102. Marguet D, Lenne P-F, Rigneault H, He H-T. Dynamics in the plasma membrane: how to combine fluidity and order. *EMBO J.* 2006;25(15):3446–57.
103. Lenne P-F, Wawrezinieck L, Conchonaud F, et al. Dynamic molecular confinement in the plasma membrane by microdomains and the cytoskeleton meshwork. *EMBO J.* 2006;25(14):3245–56.
104. Kelly C V, Wakefield DL, Holowka DA, Craighead HG, Baird BA. Near-field fluorescence cross-correlation spectroscopy on planar membranes. *ACS Nano*. 2014;8(7):7392–404.
105. Wenger J, Conchonaud F, Dintinger J, et al. Diffusion analysis within single nanometric apertures reveals the ultrafine cell membrane organization. *Biophys. J.* 2007;92(3):913–9.
106. Edel JB, Wu M, Baird B, Craighead HG. High spatial resolution observation of single-molecule dynamics in living cell membranes. *Biophys. J.* 2005;88(6):L43-5.
107. Regmi R, Winkler PM, Flauraud V, et al. Planar Optical Nanoantennas Resolve

Cholesterol-Dependent Nanoscale Heterogeneities in the Plasma Membrane of Living Cells. *Nano Lett.* 2017;17(10):.

108. Bernard A, Renault JP, Michel B, Bosshard HR, Delamarche E. Microcontact Printing of Proteins. *Adv. Mater.* 2000;12(March 2008):1067–1070.
109. Diez-Ahedo R, Normanno D, Esteban O, et al. Dynamic Re-organization of Individual Adhesion Nanoclusters in Living Cells by Ligand-Patterned Surfaces. *Small*. 2009;5(11):1258–1263.
110. Mayya V, Judokusumo E, Abu Shah E, et al. Durable Interactions of T Cells with T Cell Receptor Stimuli in the Absence of a Stable Immunological Synapse. *Cell Rep.* 2018;22(2):340–349.
111. Springer TA, Dustin ML. Integrin inside-out signaling and the immunological synapse. *Curr. Opin. Cell Biol.* 2012;24(1):107–115.
112. Grakoui A, Bromley SK, Sumen C, et al. The immunological synapse: a molecular machine controlling T cell activation. *Science (80-. ).* 1999;285(5425):221–7.
113. Lub M, van Kooyk Y, Figdor CG. Ins and outs of LFA-1. *Immunol. Today*. 1995;16(10):479–83.
114. van Kooyk Y, van de Wiel-van Kemenade P, Weder P, Kuijpers TW, Figdor CG. Enhancement of LFA-1-mediated cell adhesion by triggering through CD2 or CD3 on T lymphocytes. *Nature*. 1989;342(6251):811–3.
115. Kürzinger K, Reynolds T, Germain RN, et al. A novel lymphocyte function-associated antigen (LFA-1): cellular distribution, quantitative expression, and structure. *J. Immunol.* 1981;127(2):596–602.
116. Marlin SD, Springer TA. Purified intercellular adhesion molecule-1 (ICAM-1) is a ligand for lymphocyte function-associated antigen 1 (LFA-1). *Cell*. 1987;51(5):813–9.
117. Makgoba MW, Sanders ME, Ginther Luce GE, et al. ICAM-1 a ligand for LFA-1-dependent adhesion of B, T and myeloid cells. *Nature*. 1988;331(6151):86–8.
118. Schumann K, Lämmermann T, Bruckner M, et al. Immobilized chemokine fields and soluble chemokine gradients cooperatively shape migration patterns of dendritic cells. *Immunity*. 2010;32(5):703–13.
119. Weber M, Hauschild R, Schwarz J, et al. Interstitial Dendritic Cell Guidance by Haptotactic Chemokine Gradients. *Science (80-. ).* 2013;339(6117):328–332.
120. Gunn MD, Kyuwa S, Tam C, et al. Mice lacking expression of secondary lymphoid organ chemokine have defects in lymphocyte homing and dendritic cell localization. *J. Exp. Med.* 1999;189(3):451–60.
121. Förster R, Davalos-Misslitz AC, Rot A. CCR7 and its ligands: balancing immunity and tolerance. *Nat. Rev. Immunol.* 2008;8(5):362–71.
122. Yoshida R, Nagira M, Kitaura M, et al. Secondary lymphoid-tissue chemokine is a functional ligand for the CC chemokine receptor CCR7. *J. Biol. Chem.* 1998;273(12):7118–22.
123. Bakker GJ, Eich C, Torreno-Pina JA, et al. Lateral mobility of individual integrin nanoclusters orchestrates the onset for leukocyte adhesion. *Proc. Natl. Acad. Sci.* 2012;109(13):4869–4874.
124. Cairo CW, Mirchev R, Golan DE. Cytoskeletal regulation couples LFA-1 conformational changes to receptor lateral mobility and clustering. *Immunity*. 2006;25(2):297–308.
125. Hemmings L, Rees DJ, Ohanian V, et al. Talin contains three actin-binding sites each of which is adjacent to a vinculin-binding site. *J. Cell Sci.* 1996;109 ( Pt 11):2715–26.
126. García-Alvarez B, de Pereda JM, Calderwood DA, et al. Structural determinants of integrin recognition by talin. *Mol. Cell*. 2003;11(1):49–58.
127. Wegener KL, Partridge AW, Han J, et al. Structural Basis of Integrin Activation by Talin. *Cell*. 2007;128(1):171–182.
128. Rossier O, Octeau V, Sibarita J-B, et al. Integrins β1 and β3 exhibit distinct dynamic nanoscale organizations inside focal adhesions. *Nat. Cell Biol.* 2012;14(10):1057–67.

129. Tadokoro S, Shattil SJ, Eto K, et al. Talin Binding to Integrin Tails: A Final Common Step in Integrin Activation. *Science (80-. ).* 2003;302(5642):103–106.
130. Ginsberg MH, Partridge A, Shattil SJ. Integrin regulation. *Curr. Opin. Cell Biol.* 2005;17(5):509–16.
131. van den Dries K, van Helden SFG, Riet J te, et al. Geometry sensing by dendritic cells dictates spatial organization and PGE2-induced dissolution of podosomes. *Cell. Mol. Life Sci.* 2012;69(11):1889–1901.
132. Sampath R, Gallagher PJ, Pavalko FM. Cytoskeletal interactions with the leukocyte integrin beta2 cytoplasmic tail. Activation-dependent regulation of associations with talin and alpha-actinin. *J. Biol. Chem.* 1998;273(50):33588–94.
133. Kim M, Carman C V, Springer TA. Bidirectional Transmembrane Signaling by Cytoplasmic Domain Separation in Integrins. *Science (80-. ).* 2003;301(5640):1720–1725.